AD NUMBER

AD891403

NEW LIMITATION CHANGE

TO

Approved for public release, distribution unlimited

FROM

Distribution authorized to U.S. Gov't. agencies only; Test and Evaluation; 23 JUN 1971. Other requests shall be referred to Air Force Flight Dynamics Lab., Wright-Patterson AFB, OH 45433.

AUTHORITY

AFFDL ltr, 13 Mar 1981

AFFDL-TR-71-5
PART I, VOL I

SUBSONIC UNSTEADY AERODYNAMICS FOR GENERAL CONFIGURATIONS

PART I, VOL I—DIRECT APPLICATION OF THE NONPLANAR DOUBLET-LATTICE METHOD

J. P. GIESING
T. P. KALMAN
W. P. RODDEN

TECHNICAL REPORT AFFDL-TR-71-5, PART I, VOL I

NOVEMBER 1971

AIR FORCE FLIGHT DYNAMICS LABORATORY
AIR FORCE SYSTEMS COMMAND
WRIGHT-PATTERSON AIR FORCE BASE, OHIO

NOTICE

When Government drawings, specifications, or other data are used for any purpose other than in connection with a definitely related Government procurement operation, the United States Government thereby incurs no responsibility nor any obligation whatsoever; and the fact that the government may have formulated, furnished, or in any way supplied the said drawings, specifications, or other data, is not to be regarded by implication or otherwise as in any manner licensing the holder or any other person or corporation, or conveying any rights or permission to manufacture, use, or sell any patented invention that may in any way be related thereto.

Copies of this report should not be returned unless return is required by security considerations, contractual obligations, or notice on a specific document.

AIR FORCE: 17-12-71/150

SUBSONIC UNSTEADY AERODYNAMICS FOR GENERAL CONFIGURATIONS

PART I, VOL I—DIRECT APPLICATION OF THE NONPLANAR DOUBLET-LATTICE METHOD

J. P. GIESING
T. P. KALMAN
W. P. RODDEN

FOREWORD

This report was prepared by the Douglas Aircraft Company, Long Beach, California, for the Aerospace Dynamics Branch, Vehicle Dynamics Division, Air Force Flight Dynamics Laboratory, Wright-Patterson Air Force Base, Ohio, under Contract F33615-70-C-1167. This research was conducted under Project 1370, "Dynamic Problems in Military Flight Vehicles," and Task 137003, "Prevention of Dynamic Aeroelastic Instabilities in Advanced Military Aircraft." Mr. S. J. Pollock of the Aerospace Dynamics Branch was Task Engineer.

This report consists of two parts with two volumes for each part. This volume, Volume I of Part I is the method of direct application of nonplanar lifting surface elements. Volume I of Part II, contains a method which uses an image system and an axial singularity system to account for the effects of the bodies. Volume II of Part I is the Computer Program H7WC and Volume II of Part II is the Computer Program N5KA. The volumes containing the computer programs are available upon request from the Air Force Flight Dynamics Laboratory/FY, Wright-Patterson AFB, Ohio 45433.

The work reported herein was conducted during the period of December 1969 to September 1970.

The Principal Investigator was Joseph P. Giesing. Mrs. Terez P. Kalman was responsible for implementing the method on the computer. Donald H. Larson aided in this implementation and acted as consultant for computer problems. Dr. William P. Rodden, a McDonnell Douglas Company Consultant, contributed many valuable ideas to the project. Others have made significant contributions to this project including Messrs. D. S. Warren and W. E. Henry.

The report was submitted by the authors in November 1970 for publication as an AFFDL Technical Report.

This technical report has been reviewed and is approved.

Walter J. Mykytow

WALTER J. MYKYTOW
Asst. for Research & Technology
Vehicle Dynamics Division

ABSTRACT

Two methods of accounting for body-lifting surface interference in unsteady flow are considered. The first method is described in Part I of this report, while the second will be described in Part II to follow.

The first method is a direct application of nonplanar lifting surface elements to both the lifting surfaces and the body surfaces. The body is treated as an annular wing. This type of idealization must be used with an axial doublet introduced to account for body incidence effects. The undesirable effects of the annular wing representation are then reduced.

The second approach, to be described in Part II, uses an image system and an axial singularity system to account for the effects of the bodies.

This report also describes an improvement of the Doublet-Lattice Method of Albano and Rodden. The improvement pertains to wing-tail problems where there exists a small vertical (non-zero) separation between the wing and tail planes. Such problems can now be handled with ease.

This volume contains the development of the theory, correlation of theory with experimental data, and the parametric study. Volume II is a guide to the computer program and contains the FORTRAN listing.

CONTENTS

		Page
1.0	INTRODUCTION	1
2.0	THEORETICAL DEVELOPMENT	2
2.1	The Doublet-Lattice Method	2
2.1.1	Integration Over an Element	4
2.1.2	Reflection Planes and Ground Effect	10
2.2	Lifting-Surface/Body Interference	13
2.2.1	Slender Body Force Distributions and Their Resulting Flow Fields	14
2.2.2	Interference	18
2.3	The Normalwash Boundary Conditions	21
2.4	Loads and Forces	23
2.4.1	Generalized Forces	23
2.4.2	Aerodynamic Parameters	24
2.5	Aerodynamic Influence Coefficients and Harmonic Gust Coefficients	28
2.5.1	General Considerations	28
2.5.2	The Substantial Derivative Matrix	30
2.5.3	The Integration Matrix	32
2.6	Matrix Solution	34
3.0	CALCULATED RESULTS	36
3.1	Convergence of Results	36
3.2	Nearly Coplanar Wing-tail Configuration	37
3.3	Wing-Body Combinations	37
3.4	Conclusions	41
	REFERENCES	49

CONTENTS (Cont.)

		Page
APPENDIX A	The Kernel Function for Lifting Surfaces	51
APPENDIX B	Integration over an Element	57
APPENDIX C	The Steady Nonplanar Downwash Factor	61
APPENDIX D	The Substantial Derivative and Integration Matrices.	70

NOMENCLATURE

A	Reference total area
$\lceil A \rfloor$	Matrix of box areas
a_{inm}	Polynomial mode coefficients for mode i
AIC	Matrix of influence coefficients relating generalized forces to generalized deflections for submodes
c	Chord length
$\bar{c}$	Reference chord length
C_m	Pitching moment coefficient $\left(\frac{\text{moment}}{q\ A\bar{c}}\right)$, (+ nose up)
C_n	Yawing moment coefficient $\left(\frac{\text{moment}}{q\ A\ s}\right)$ (+ nose right)
C_ℓ	Rolling moment coefficient $\left(\frac{\text{moment}}{q\ As}\right)$ (+ clockwise)
C_Y	Force coefficient in y-direction $\left(\frac{\text{Force}}{q\ A}\right)$ (+ out right wing)
C_Z	Force coefficient in z-direction $\left(\frac{\text{Force}}{q\ A}\right)$ (+ vertically up)
c_m	Local moment coefficient $\left(\frac{\text{moment}}{q\ c^2}\right)$
c_n	Local normal force coefficient $\left(\frac{\text{normal force}}{qc}\right)$
e	Strip semi-width
f	Normalized deflection normal to surface (h/s)
h	Deflection normal to surface
K	Kernel
k_r	Reduced frequency, $\omega\bar{c}/2U_\infty$
L	Lift
M	Mach number;also moment
Q_{ij}	Generalized force
q	Dynamic pressure
$\bar{q}$	Generalized coordinates
R_o	Body radius
r	$\sqrt{(y-\eta)^2 + (z-\zeta)^2}$

s	Semi-span
U_∞	Free-stream velocity
W	Unnormalized normalwash
w	W/U_∞
wr	$w - w_b$
x, y, z	Coordinates of receving points
$\bar{x}, \bar{y}, \bar{z}$	Element coordinates of receiving points
x_o	Gust reference axis
α	Angle of attack; also a function defined by Equation 2.1-15
β	$\sqrt{1 - M^2}$; also control surface deflection
Γ_g	Gust dihedral angle. ($\Gamma_g = 0$ if gust velocity is vertical)
γ	Dihedral angle
ΔC_p	Lifting pressure coefficient $\frac{P_{lower} - P_{upper}}{q}$
δ	Symmetry index (right and left symmetry); also tab deflection
ϵ	Ground effect index
λ	Wave length
ξ, η, ζ	Coordinates of sending points
$\bar{\xi}, \bar{\eta}, \bar{\zeta}$	Coordinates of sending points in element coordinates
ρ_o	Density at sea level
σ	Lateral coordinate in the plane of the surface
ω	Frequency

Subscripts and Superscripts

a	body axis
B	body
c	center
f	Body or fuselage
g	gust

i	Deflection mode
j	Pressure mode
L. E.	Leading edge
LL	Lower left
LR	Lower right
R	Axis about which moments are taken
r	Receiving
s	Sending
UL	Upper left
UR	Upper right
y	y-direction
z	z-direction
1/4	One quarter chord point of a lifting surface box
3/4	Three quarters chord point of a lifting surface box

1.0 INTRODUCTION

This report presents a direct application of the Doublet-Lattice Method to problems involving body-lifting surface interference. The Doublet-Lattice Method of Albano and Rodden[1] which is used here, is an extension of the steady Vortex-Lattice Method. Developments by Hedman,[2] Giesing,[3] and James[4] have shown that the Vortex-Lattice Method is (1) simple (2) accurate and (3) quite versatile. Correlations by Kalman, Rodden and Giesing[5] show that the same attributes apply to the unsteady Doublet-Lattice Method. A survey of the development of the steady and unsteady lattice methods is given in Reference 5.

Two methods of accounting for body-lifting surface interference in unsteady flow are considered. The first method is described in Part I of this report, while the second will be described in Part II to follow.

The first method is a direct application of nonplanar lifting surface elements to both the lifting surfaces and the body surfaces. The body is treated as an annular wing. Such an idealization has been used by Woodward[6] in the steady case. This type of idealization must be used with an axial doublet introduced to account for body incidence effects. The undesirable effects of the annular wing representation are then reduced.

The second approach, to be described in Part II, uses an image system and an axial singularity system to account for the effects of the bodies. Basically it will be an extension of the method of Reference 3.

This report also describes an improvement of the Doublet-Lattice Method of Albano and Rodden. The improvement pertains to wing-tail problems where there exists a small vertical (non-zero) separation between the wing and tail planes. Such problems can now be handled with ease.

2.0 THEORETICAL DEVELOPMENT

2.1 The Doublet-Lattice Method

The velocity normal to an oscillating surface, $W = U_\infty \, Re\left(w \, e^{i\omega t}\right)$, is related to the lifting pressure $\Delta p = q \, Re\left(\Delta C_p \, e^{i\omega t}\right)$, by the integral equation

$$w(x, y, z) = \frac{1}{8\pi} \iint_{L.S.} K(x-\xi, \; y-\eta, \; z-\zeta, \omega, \; M) \; \Delta C_{\bar{p}} \; d\xi \; \; d\sigma \qquad (2.1\text{-}1)$$

where ξ is the streamwise coordinate, σ is the tangential spanwise coordinate (see Sketch 2.1-1), ω is the frequency of oscillation, M is the Mach Number and K is the kernel. The limit L. S. indicates integration over all the lifting surfaces. The integral in Eq. (2.1-1) can be approximated as follows:

$$w(x, y, z) = \frac{1}{8\pi} \sum_s \Delta C_{p_s} \iint_{Element_s} K(x-\xi, \; y-\eta, \; z-\zeta, \omega, \; M) \, d\xi \, d\sigma \qquad (2.1\text{-}2)$$

where s is an index indicating the sending element A further approximation is introduced in the Vortex- and Doublet-Lattice Methods. The integration of K in the streamwise direction (ξ) is done simply by lumping the effect into

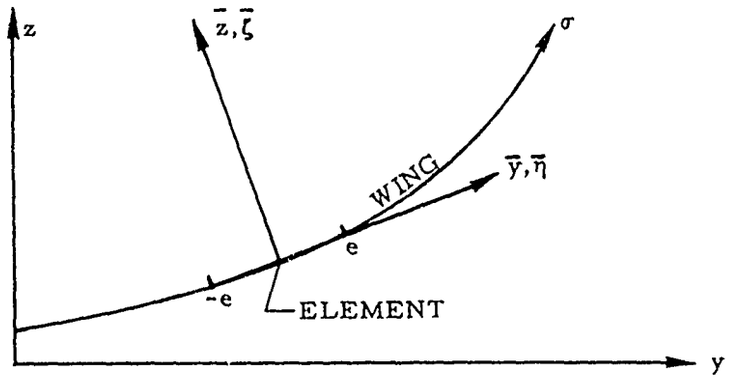

SKETCH 2.1-1 WING AND ELEMENT COORDINATES

a loaded line at the 1/4-chord line of the element.

$$w(x, y, z) = \sum_s \Delta C_{p_s} \frac{\Delta \xi}{8\pi} \int_{\text{Element}_s} K(x-\xi_{1/4}, y-\eta, z-\zeta, \omega, M)\, d\sigma \quad (2.1\text{-}3)$$

The result is an unsteady horseshoe vortex whose bound portion lies along the 1/4-chord line of the element.

In this equation the normalwash boundary condition $w(x, y, z)$ is known and the lifting pressure, ΔC_{p_s}, over each element is unknown. A set of linear algebraic equations may be formed from (2.1-3) if the normalwash is satisified at as many points as there are elements. Equation (2.1-3) can then be written in matrix form

$$\{w\} = [D] \{\Delta C_p\} \quad (2.1\text{-}4)$$

where a typical element of $[D]$, D_{rs}, is

$$D_{rs} = \int_{\text{Element}_s} K(x-\xi_{1/4}, y-\eta, z-\zeta, \omega, M)\, d\sigma \quad (2.1\text{-}5)$$

and where x, y, z (both for D_{rs} and w_r) are the coordinates of the receiving point "r". There is one control or receiving point per element and the surface normalwash boundary condition is satisfied at each of these points. The control point is centered spanwise on the three-quarter chord line of the element (Sketch 2.1-2). This choice of control point location, shown by James[4] to be optimum for the two-dimensional case, results in a high degree of accuracy. Sketch 2.1-2 also shows the idealization of the surface into elements or boxes which are arranged in strips parallel to the free stream so that surface edges, fold lines, and hinge lines lie on element or box boundaries.

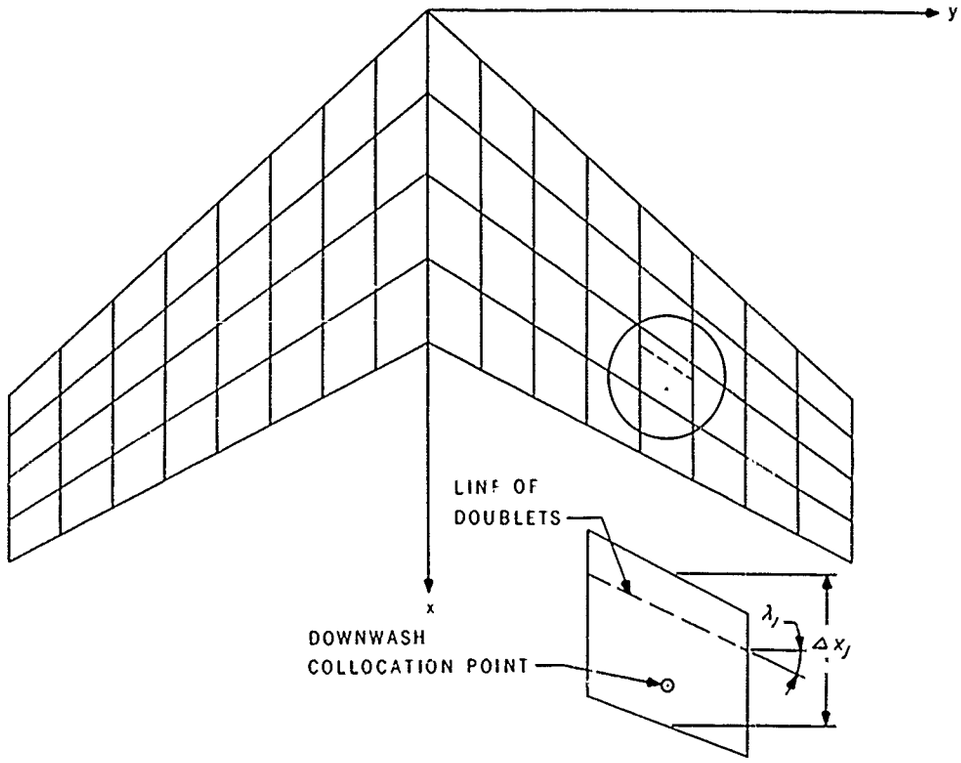

Sketch 2.1-2. Idealization of a Wing Panel into Boxes

2.1.1 Integration Over an Element

The general form of the nonplanar kernel, K, used is given by Rodemich[7] and Landahl[8] as:

$$K = e^{-i\frac{\omega}{U_\infty}(x-\xi)} (K_1 T_1 + K_2 T_2)/r^2 \qquad (2.1\text{-}6)$$

where K_1, T_1, K_2, and T_2 are given in Appendix A. The basic idea of the Doublet-Lattice Method is to fit the numerator of K with a parabola and integrate (2.1-5) analytically. Since the steady kernel can be integrated exactly without the parabolic fit it is apparent that the accuracy will be improved if only the unsteady increment is integrated using the approximating

parabola. Equation (2.1-6) becomes

$$K(x-\xi_{1/4},\ y-\eta,\ z-\zeta,\ \omega,\ M) =$$

$$\left\{T_1\left[e^{-i\frac{\omega}{U_\infty}(x-\xi_{1/4})}K_1\text{-}K_1^{(s)}\right] + T_2\left[e^{-i\frac{\omega}{U_\infty}(x-\xi_{1/4})}K_2\text{-}K_2^{(s)}\right]\right\}\Big/ r^2$$

$$+ \left\{T_1 K_1^{(s)} + T_2 K_2^{(s)}\right\}/r^2 \qquad (2.1\text{-}7)$$

The superscript "s" indicates the steady case ($\omega = 0$). The first of the bracketed terms in the numerator of Equation (2.1-7) is fitted with a parabola and integrated while the second of the bracketed terms is integrated analytically without the use of a curve fit.

$$D_{rs} = D_{rs}^{(1)} + D_{rs}^{(s)} \qquad (2.1\text{-}8)$$

where

$$D_{rs}^{(1)} = \frac{\Delta\chi_s}{8\pi}\int_{-e}^{e}\frac{A\bar{\eta}^2 + B\bar{\eta} + C}{r^2}\,d\bar{\eta}$$

$$D_{rs}^{(s)} = \frac{\Delta\chi_s}{8\pi}\int_{-e}^{e}\left\{T_1 K_1^{(s)} + T_2 K_2^{(s)}\right\}\frac{d\bar{\eta}}{r^2}$$

and where $A\bar{\eta}^2 + B\bar{\eta} + C = T_1\left[e^{-i\frac{\omega}{U_\infty}(x-\xi_{1/4})}K_1\text{-}K_1^{(s)}\right] + T_2\left[e^{-i\frac{\omega}{U_\infty}(x-\xi_{1/4})}K_2\text{-}K_2^{(s)}\right]$

Here "e" is the semi-width of the element in the plane of the element. The integration involved in $D_{rs}^{(1)}$ is shown in Appendix B. The term $D_{rs}^{(s)}$ represents a steady horseshoe vortex and its evaluation is given in Appendix C The change in variable from σ to $\bar{\eta}$ indicates that element coordinates are to

be used. (See Sketch 2.1-1) Element coordinates for a particular element are centered on the sending element and rotated into the plane of the element. The relations between element coordinates and the usual coordinates are given as:

$$\bar{x} = x - \xi_c$$

$$\bar{y} = (y - \eta_c)\cos\gamma_s + (z - \zeta_c)\sin\gamma_s$$

$$\bar{z} = (z - \zeta_c)\cos\gamma_s - (y - \eta_c)\sin\gamma_s$$

$$\bar{\gamma}_r = \gamma_r - \gamma_s$$

where ξ_c, η_c and ζ_c are the coordinates of the center of the 1/4-chord line of the sending element and γ_s is the dihedral angle of the element. The expressions for $\bar{\xi}$, $\bar{\eta}$, and $\bar{\zeta}$ are the same as above with x, y and z replaced with ξ, η and ζ.

The integration used to obtain $D_{rs}^{(1)}$ works very well for all cases, planar and nonplanar, with one exception. Consider the case where the receiving point is downstream of the sending element. When there exists a small vertical separation between the receiving point and sending element then the numerator of the kernel has large variations with $\bar{\eta}$ and a parabolic fit will not give accurate results.

The problem can best be understood by considering the nature of the kernel. It can be shown that the kernel is a semi-infinite line doublet whose strength varies like $\exp[-i\omega(\xi - \xi_{1/4})/U_\infty]$ aft of the point $\xi_{1/4}$. This semi-infinite line doublet is to be integrated in the $\bar{\eta}$-direction (spanwise in the plane of the element). When the receiving point is downstream of the sending point of the kernel with a small vertical and lateral gap, i.e., small $\bar{z}$ and $\bar{y}$, then the flow field is dominated by the local strength of the semi-infinite doublet line.

Expressions for the various parts of the kernel valid for small lateral distances, and downstream of the sending point, in element coordinates, are:

$$\lim_{\beta^2 r/(x-\xi_{1/4}) \to 0} \qquad x > \xi_{1/4} \quad \text{when} \quad r^2 = (\bar{y}-\bar{\eta})^2 + \bar{z}^2$$

$$K_1 \to 2 \qquad K_2 \to -4$$

$$T_1 = \cos \bar{\gamma}_r$$

$$T_2 = \left(\bar{z}^2/r^2\right)\cos\bar{\gamma}_r - \left(\bar{z}(\bar{y}-\bar{\eta})/r^2\right)\sin\gamma_r \qquad (2.1\text{-}9)$$

These terms may be used to construct the unsteady increment given by the first term in brackets on the right-hand-side of Equation (2.1-7). The numerator of this term is to be fit with a parabola. Investigation of the variation of this term with $\bar{\eta}$ will show why a parabola is inadequate and it will also suggest a way to remedy the situation.

Using Equation (2.1-9) above in the numerator gives:

$$\lim_{\beta^2 r/(x-\xi_{1/4}) \to 0} \left\{ T_1 \left[e^{-i\frac{\omega}{U_\infty}(x-\xi_{1/4})} K_1 - K_1^{(s)} \right] + T_2 \left[e^{-i\frac{\omega}{U_\infty}(x-\xi_{1/4})} K_2 - K_2^{(s)} \right] \right\} \to$$

$$\to \left\{ e^{-i\frac{\omega}{U_\infty}(x-\xi_{1/4})} - 1 \right\} \left\{ 2\cos\bar{\gamma}_r - 4\cos\bar{\gamma}_r \frac{\bar{z}^2}{r^2} + 4\sin\bar{\gamma}_r \frac{\bar{z}(\bar{y}-\bar{\eta})}{r^2} \right\} \qquad (2.1\text{-}10)$$

The terms that cause the trouble arise from the nonplanar term and are the ones that are divided by r^2. Plots of $\bar{z}^2/r^2$ and $-\bar{z}(\bar{y}-\bar{\eta})/r^2$ (when $\bar{y}$ is zero) are given in Sketch (2.1-3).

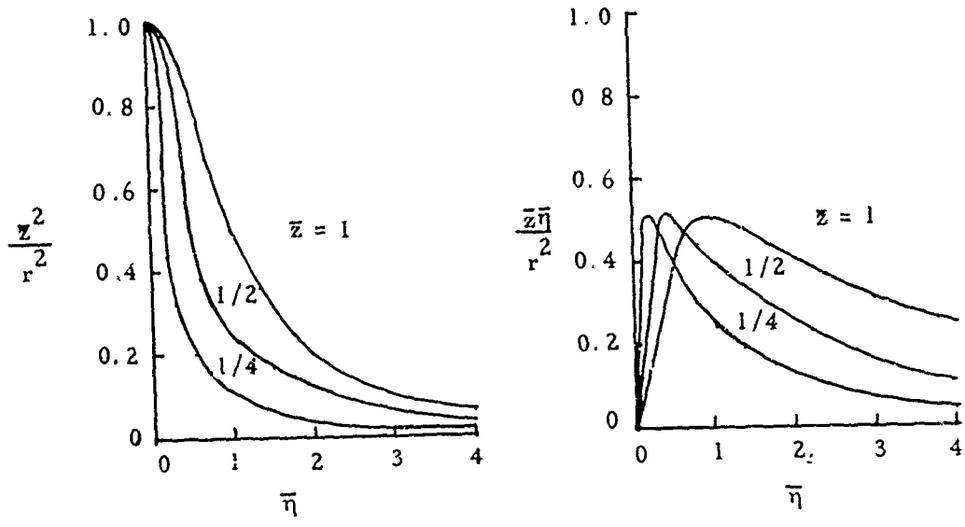

SKETCH 2.1-3

When the element length, 2e, is large compared with $\bar{z}$ the variations across the element are very large and a parabola is inadequate.

The obvious solution to this problem is to consider the nonplanar terms separately from the planar. The nonplanar terms have basically a different behavior than the planar terms. The planar terms vary like $1/r^2$ but the nonplanar terms vary like $1/r^4$. This suggests that the kernel should be written as:

$$K = e^{-i\frac{\omega}{U_\infty}(x-\xi_{1/4})}(K_1 T_1/r^2 + K_2 T_2^*/r^4) \qquad (2.1\text{-}11)$$

where

$$T_2^* = r^2 T_2^2 = [(z-\zeta)\cos\gamma_r - (y-\eta)\sin\gamma_r][(z-\zeta)\cos\gamma_s - (y-\eta)\sin\gamma_s)$$

Again the steady kernel should be considered separately to increase the accuracy.

$$K = \left\{ T_1 \left[e^{-i\frac{\omega}{U_\infty}(x-\xi_{1/4})} K_1 - K_1^{(s)} \right] / r^2 + T_2^* \left[e^{-i\frac{\omega}{U_\infty}(x-\xi_{1/4})} K_2 - K_2^{(s)} \right] / r^4 \right\}$$

$$+ \left\{ T_1 K_1^{(s)} / r^2 + T_2^* K_2^{(s)} / r^4 \right\} \qquad (2.1\text{-}12)$$

Of course, the steady kernel is integrated separately to a steady horseshoe vortex. The numerators of each of the terms in the first bracket may now each be fit with a parabola since they are very slowly varying functions of $\bar{\eta}$ across an element.

$$T_1 \left[e^{-i\frac{\omega}{U_\infty}(x-\xi_{1/4})} K_1 - K_1^{(s)} \right] \approx A_1 \bar{\eta}^2 + B_1 \bar{\eta} + C_1$$

$$T_2^* \left[e^{-i\frac{\omega}{U_\infty}(x-\xi_{1/4})} K_2 - K_2^{(s)} \right] \approx A_2 \bar{\eta}^2 + B_2 \bar{\eta} + C_2 \qquad (2.1\text{-}13)$$

Equation (2.1-5) then becomes:

$$D_{rs} = D_{rs}^{(1)} + D_{rs}^{(2)} + D_{rs}^{(s)} \qquad (2.1\text{-}14)$$

where

$$D_{rs}^{(1)} = \int_{-e}^{e} \frac{A_1 \bar{\eta}^2 + B_2 \bar{\eta} + C_1}{r^2} \, d\bar{\eta}$$

$$D_{rs}^{(2)} = \int_{-e}^{e} \frac{A_2 \bar{\eta}^2 + B_2 \bar{\eta} + C_2}{r^4} \, d\bar{\eta}$$

$$D_{rs}^{(s)} = \int_{-e}^{e} (T_1 K_1^{(s)} / r^2 + T_2^* K_2^{(s)} / r^4) \, d\bar{\eta}$$

The integrals $D_{rs}^{(1)}$ and $D_{rs}^{(s)}$ are the same as those encountered in Equation (2.1-8) except that the coefficients A, B, C in (2.1-8) are not the same as

A_1, B_1, and C_1 in (2.1-13). The term $D_{rs}^{(2)}$ is new and represents the nonplanar unsteady increment. The evaluation of $D_{rs}^{(2)}$ is given in Appendix II. The final expression is:

$$D_{rs}^{(2)} = \frac{(e/2)\Delta\xi}{(\bar{y}^2+\bar{z}^2-e^2)} \left\{ \frac{2(\bar{y}^2+\bar{z}^2+e^2)(A_2e^2+C_2)+4\bar{y}e^2B_2}{[(\bar{y}+e)^2+\bar{z}^2][(\bar{y}-e)^2+\bar{z}^2]} \right.$$

$$\left. - \frac{\alpha}{e^2}\left[(\bar{y}^2+\bar{z}^2)A_2+\bar{y}B_2+C_2\right] \right\} \qquad (2.1\text{-}15)$$

where

$$\alpha = \frac{e^2}{\bar{z}^2}\left[1 - \frac{(\bar{y}^2+\bar{z}^2-e^2)}{2e|\bar{z}|}\tan^{-1}\left\{\frac{2e|\bar{z}|}{(\bar{y}^2+\bar{z}^2-e^2)}\right\}\right]$$

Appendix B gives an expansion for α valid for small values of $\bar{z}$ and an equation valid for small values of $\bar{y}^2 + \bar{z}^2 - e^2$.

2.1.2 Reflection Planes and Ground Effect

Most applications of the present method involve configurations with one or two planes of symmetry. The X-Z plane is a plane of symmetry for most cases, e.g., the right side of a lifting surface is the mirror image of the left side. In other cases an additional plane of symmetry (the X-Y plane) exists. For instance a lifting surface attached to a ground plane (as in a wind tunnel) or in the proximity of the ground (aircraft in ground effect) represents a configuration with two planes of symmetry.

All flow conditions can be split up into symmetrical and/or antisymmetrical parts in relation to either plane of symmetry. If the configuration is symmetrical and the flow is either symmetrical or antisymmetrical then a considerable savings in computational effort can be realized. Consider the general case of two planes of symmetry. The

entire lifting surface system is made up of segments in the upper right (UR) quadrant, the upper left (UL), the lower right (LR) and the lower left (LL). If the distribution of lifting pressure and normalwash are each split into their component segments (one per quadrant) and so designated by the subscripts UR, UL, LR and LL the matrix equation given by Eq. 2.1-4 can be written as:

$$\begin{Bmatrix} w_{UR} \\ w_{UL} \\ w_{LR} \\ w_{LL} \end{Bmatrix} = \begin{bmatrix} d_{11} & d_{12} & d_{13} & d_{14} \\ d_{21} & d_{22} & d_{23} & d_{24} \\ d_{31} & d_{32} & d_{33} & d_{34} \\ d_{32} & d_{33} & d_{34} & d_{35} \end{bmatrix} \begin{Bmatrix} \Delta C_{pUR} \\ \Delta C_{pUL} \\ \Delta C_{pLR} \\ \Delta C_{pLL} \end{Bmatrix} \quad (2.1\text{-}16)$$

where d_{ij} are submatrices of D_{ij}.

Let the flow symmetry betweer right and left be indicated by the term

$$\delta = \begin{cases} 1 \text{ symmetry} \\ -1 \text{ antisymmetry} \\ 0 \text{ no symmetry} \end{cases}$$

In addition let ϵ indicate symmetry between upper and lower.

$$\epsilon = \begin{cases} 1 \text{ symmetry} \\ -1 \text{ antisymmetry (ground effect)} \\ 0 \text{ no symmetry} \end{cases}$$

Then $\Delta C_{pUL} = \delta \Delta C_{pUR}$

$$\Delta C_{pLR} = \epsilon \Delta C_{pUR} \qquad (2.1\text{-}17)$$

$$\Delta C_{pLL} = \delta \Delta C_{pLR} = \delta\epsilon \Delta C_{pUR}$$

The distributions for all of the quadrants have been reduced to one distribution for the upper right quadrant ΔC_{pUR}. Using (2.1-17) in (2.1-16) gives

$$w_{UR} = \left[d_{11} + \delta d_{12} + \epsilon d_{13} + \epsilon\delta d_{14} \right] \left\{ \Delta C_{pUR} \right\}$$

Thus only that part of the configuration that appears in the upper right hand quadrant needs to be considered.

Configurations such as T-tails present no special problems; however, the results obtained by the present method for these cases must be properly interpreted. The vertical surface of the T-tail is in reality two surfaces. Consider the configuration in Sketch 2.1-4.

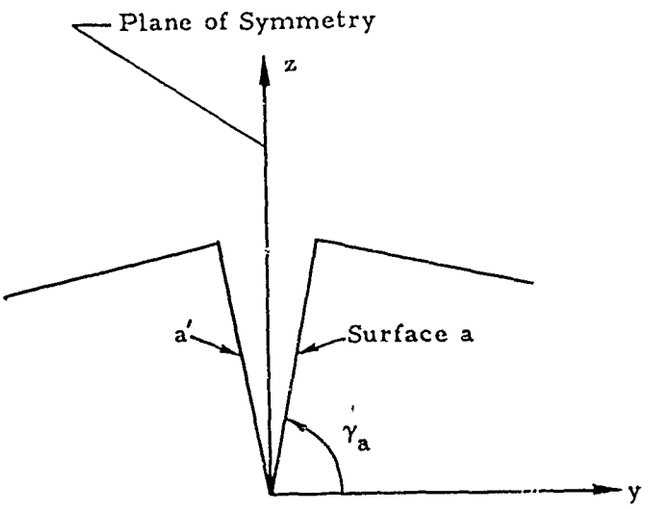

Sketch 2.1-4. Symmetry considerations for T-tails

The T-tail is formed in the limit as the dihedral of surface "a" (γ_a) approaches 90°. The vertical fin is then made up of surface "a" plus its reflection a'. The present method determines the loading only on surfaces in the right hand sector and thus only half of the loading is determined for the vertical fin. The lifting pressure distribution and the spanwise loading and moment are off by a factor of two. (Program H7WC tests for this condition and adjusts these distributions. See Vol II) The image lifting surface is always accounted for when calculating stability derivatives or generalized forces. Since the vertical fin surface "a" has an image a' the derivatives are calculated correctly. When dealing with aeroelastic problems the structure is always cut in half along a symmetry plane. This cut splits the vertical fin of a T-tail into two equal surfaces. Only half of the aerodynamic forces are applied to each half of the fin. Thus the AIC calculation, to be described in Section 2.5 for use in aeroelastic problems, is formed properly by the present method.

2.2 Lifting-Surface/Body Interference

The treatment of lifting-surface/body combinations presented in this report (Part I) is similar to that of Woodward[6]. Woodward considered only the steady case for a single body whereas the more general oscillatory case for multiple bodies is dealt with here. The effects of the isolated bodies are obtained using slender body theory. Body-lifting surface interference is obtained by placing lifting surface elements on the body surface near the body-lifting surface intersection.

The order of solution again is similar to that employed by Woodward. The slender body solution for the longitudinal force distribution on all bodies is obtained first. The slender body solution used (J. W. Miles[9]) handles bodies of circular cross-section whose radius varies in the longitudinal direction. The motion of the body may be arbitrary. The longitudinal force distribution on the bodies causes a flow field which affects the lifting surface elements. The normalwash due to this flow field is then determined at all lifting surface elements <u>except</u> those on the body surfaces. The axial singularities found for a single isolated body using the slender body theory

divert the flow around that body. The resulting values of normalwash found at the interference lifting surface elements, for that body, are therefore zero. For the case of several bodies there is a small nonzero normalwash caused by the singularity systems of the other bodies. Exact solutions to the unsteady compressible wave equation are used to determine the flow fields generated by the bodies. Specifically, pressure doublet distributions are used. The normalwash caused by the body axial force distributions is added to the normalwash generated by the motions of the lifting surface. The resulting boundary value problem is then solved exactly as outlined in the last Section (2.1).

2.2.1 Slender Body Force Distributions and their Resulting Flow Fields

The slender body theory of J. W. Miles[9] is used for the unsteady case. The longitudinal lift distribution for harmonic motion is given by Equation 16 of Reference 9 and is

$$\frac{\partial L}{\partial x} = \left(U_\infty \frac{\partial}{\partial x} + i\omega \right) \left(m(x)\, w^{(f)}(x) \right) e^{i\omega t} \qquad (2.2\text{-}1)$$

where m(x) is the virtual mass of the cross section and w(x) is the normalized upwash" $(W^{(f)}/U_\infty)$ in the direction of L. For a circular cross-section of radius $R_o(x)$, $m(x) = U_\infty \rho \pi R_o^2(x)$. Introduction of this value of m(x) into Equation (2.2-1) gives:

$$\frac{1}{q} \frac{\partial L}{\partial x} \frac{1}{2R_o} = \pi \left\{ 2R_o' \, w^{(f)} + R_o \, w' + i \frac{\omega R_o}{U_\infty} w^{(f)} \right\} \qquad (2.2\text{-}2)$$

The term on the left-hand-side of Equation (2.2-2) may be regarded as a lifting pressure coefficient, $\Delta C_p^{(f)}$, acting on the projected body area. The force per unit length is obtained simply as this pressure multiplied by the local body diameter and dynamic pressure.

$$\frac{\partial L}{\partial x} = q\, 2R_o \, \Delta C_p^{(f)} \qquad (2.2\text{-}3)$$

and thus from (2.2-2):

$$\Delta C_p^{(f)} = 2\pi \left\{ R_o' \; w^{(f)} + w^{(f)'} R_o/2 + ik_r \, w^{(f)} R_o/\bar{c} \right\} \qquad (2.2\text{-}4)$$

where the reduced frequency $k_r = \frac{\omega \bar{c}}{2 U_\infty}$ has been introduced.

The pressure $\Delta C_p^{(f)}$ actually acts only on the body axis and thus acts like a delta function whose integrated value is $2 R_o \Delta C_p^{(f)}$. Furthermore, $\Delta C_p^{(f)}$ has two components in general, a vertical, ΔC_Z, and a horizontal, ΔC_Y, as does the upwash to the fuselage $w^{(f)}$. Thus

$$\overrightarrow{\Delta C}_p^{(f)} = \delta(y-\eta_a, z-\zeta_a) \left\{ \Delta C_Z \vec{k} + \Delta C_Y \vec{j} \right\}$$

where η_a and ζ_a are the coordinates of the body axis. Also it can be shown that if a pressure doublet is placed within a circular body the total integrated force is 0.5 $(\Delta \overrightarrow{C_p}^{(f)} \Delta A)$; i.e., the pressure doublet is only half as effective when it lies within a circular body. Thus, if the lifting surface theory is to be used to obtain the flow field due to $\Delta \overrightarrow{C_p}^{(f)}$ then $2\Delta \overrightarrow{C_p}^{(f)}$ must be used. A slight generalization of (2.1-1) gives:

$$w_B(x,y,z) = \frac{1}{4\pi} \iint K_Z(x-\xi, y-\eta, z-\zeta, \omega, M) \; \delta(y-\eta_a, z-\zeta_a) \, \Delta C_Z \, d\xi d\eta + \frac{1}{4\pi} \iint K_Y(x-\xi, y-\eta, z-\zeta, \omega, M) \; \delta(y-\eta_a, z-\zeta_a) \, \Delta C_Y \, d\xi d\zeta \qquad (2.2\text{-}4)$$

where the subscripts Z and Y on K indicate the direction of the pressure doublet sheet, and the B subscript on w indicates that the normal wash is caused by the bodies. Integration of the delta function, δ, in the η and ζ directions gives

$$w_B(x,y,z) = \frac{1}{4\pi} \int K_Z(x-\xi, y-\eta_a, z-\zeta_a, \omega, M) \; \Delta C_Z \; 2 R_o \, d\xi + \frac{1}{4\pi} \int K_Y(x-\xi, y-\eta_a, z-\zeta_a, \omega, M) \; \Delta C_Y \; 2 R_o \, d\xi \qquad (2.2\text{-}5)$$

Integration in the longitudinal direction is done numerically. Each body axis is divided into a number of elements over which $R_o C_Y$ and $R_o C_Z$ are assumed constant.

$$w_B(x,y,z) = \frac{1}{2\pi} \sum_s \left(\Delta C_{Z_s} \; R_{o_s} \int_{\text{Element}_s} K_Z (x-\xi,\; y-\eta_a,\; z-\zeta_a, \omega,\; M)\, d\xi \right) \tag{2.2-6}$$

$$+ \frac{1}{2\pi} \sum_s \left(\Delta C_{Y_s} \; R_{o_s} \int_{\text{Element}_s} K_Y (x-\xi,\; y-\eta_a,\; z-\zeta_a, \omega,\; M)\, d\xi \right)$$

Integration over each element is done by lumping the effect at the leading edge of each element, i.e., at $\zeta = \xi_{a_s}$

$$w_B(x,y,z) = \frac{1}{2\pi} \sum \Delta C_{Z_s} \; R_{o_s} \; \Delta\xi_s \; K_{Z_s} (x-\xi_{a_s},\, y-\eta_a,\, z-\zeta_a, \omega, M) \tag{2.2-7}$$

$$+ \frac{1}{2\pi} \sum \Delta C_{Y_s} \; R_{o_s} \; \Delta\xi_s \; K_{Y_s} (x-\xi_{a_s},\, y-\eta_a,\, z-\zeta_a, \omega, M)$$

The values of the normalwash at wing (or tail, etc.) lifting surface control points and other body lifting surface control points may be assembled into a column matrix $\left\{ w_B \right\}$. Using (2.2-7) this column matrix may be written as

$$\left\{ w_B \right\} = [F_Z] \left\{ \Delta C_Z \right\} + [F_Y] \left\{ \Delta C_Y \right\} \tag{2.2-8}$$

where typical elements of the non-square matrices $[F_Z]$ and $[F_Y]$ are

$$F_{Z_{rs}} = \frac{1}{2\pi} \; R_{o_s} \; \Delta\xi_s \; K_{Z_{rs}} \tag{2.2-9}$$

$$F_{Y_{rs}} = \frac{1}{2\pi} \; R_{o_s} \; \Delta\xi_s \; K_{Y_{rs}} \tag{2.2-10}$$

where $K_{Z_{rs}} = K_Z(x-\xi_{a_s}, y-\eta_a, z-\zeta_a, \omega, M)$ and $K_{Y_{rs}} = K_Y(x-\xi_{a_s}, y-\eta_a, z-\zeta_a, \omega, M)$ are evaluated at the r^{th} receiving point whose coordinates are given by x, y, z.

Equation (2.2-8) may be written in a partitioned form as

$$\left\{ w_B \right\} = [F] \left\{ \Delta C_p^{(f)} \right\} \qquad (2.2\text{-}11)$$

where $[F] = [F_Z \vdots F_Y]$

$$\left\{ \Delta C_p^{(f)} \right\} = \begin{Bmatrix} \Delta C_{pZ} \\ \vdots \\ \Delta C_{pY} \end{Bmatrix}$$

The boundary conditions at the lifting surfaces are obtained from the motions of the surfaces. Specifically, the substantial derivative of the surface deflection produces the required normalwash velocity w. Both lifting surface and body axis singularities are introduced to produce this normal velocity. If lifting surfaces alone are considered the matrix formulation is taken from Equation (2.1-4), i.e.,

$$\left\{ w \right\} = [D] \left\{ \Delta C_p \right\}$$

When axial singularities are introduced as in the present method this formula becomes:

$$\left\{ w \right\} = [D] \left\{ \Delta C_p \right\} + [F] \left\{ \Delta C_p^{(f)} \right\} \qquad (2.2\text{-}12)$$

In this matrix equation only the boundary conditions on the lifting surfaces are considered. The matrix [D] represents the effect of lifting surfaces on themselves and is square. The matrix [F] represents the effect of the body axial singularities on the lifting surfaces and is rectangular.

Using equation (2.2-11) in (2.2-12) gives

$$\left\{wR\right\} = \left\{ w-w_B \right\} = [D] \left\{ \Delta C_p \right\} \qquad (2.2\text{-}13)$$

This is the final matrix eqution to be solved for the unknown lifting pressures $\left\{\Delta C_p\right\}$.

2.2.2 Interference

The slender body theory satisfies the boundary conditions on bodies undergoing general oscillatory motions. That is, the slender body theory satisifies the upwash and sidewash boundary conditions given by $w^{(f)}$. When lifting surfaces (or other bodies) are introduced into the flow, the body boundary conditions are no longer satisified. The region of greatest disturbance is near the body-lifting surface intersection. An initial attempt to account for this interference is presented here (Part I). The basic idea is to apply lifting surface elements directly to the body surface in regions where the body boundary condition is most seriously disturbed. Each lifting surface element possesses its own wake. Each wake trails straight back from the element in the x-direction (see Reference 10). Because of this fundamental characteristic the configurations that may be considered are limited. Specifically, placing lifting elements on the actual body surface* is not acceptable since the wakes may thread in and out of the body surface aft of the lifting element in question (see Sketch 2.2-1'). The actual wake, if any exists at all, springs from the separation regions of the body.

* Consideration of forward or rearward inclined surfaces requires a kernel of the type developed by Berman [10].

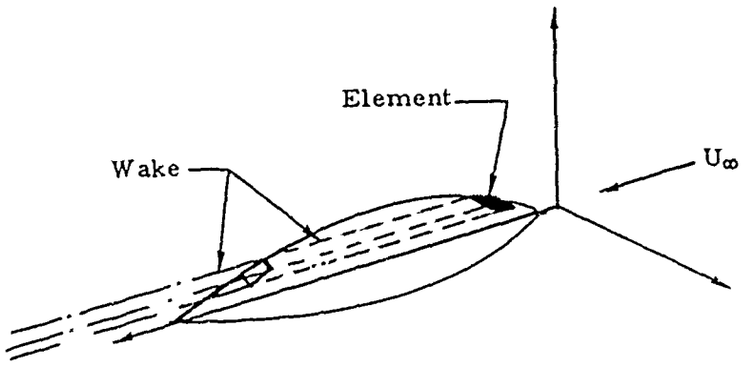

Sketch 2.2-1

The shape of that section of the body on which lifting surface elements are placed must be idealized. Specifically, the interference region of the body must have a constant cross-sectional shape. Sketch 2.2-2 presents a graphical example.

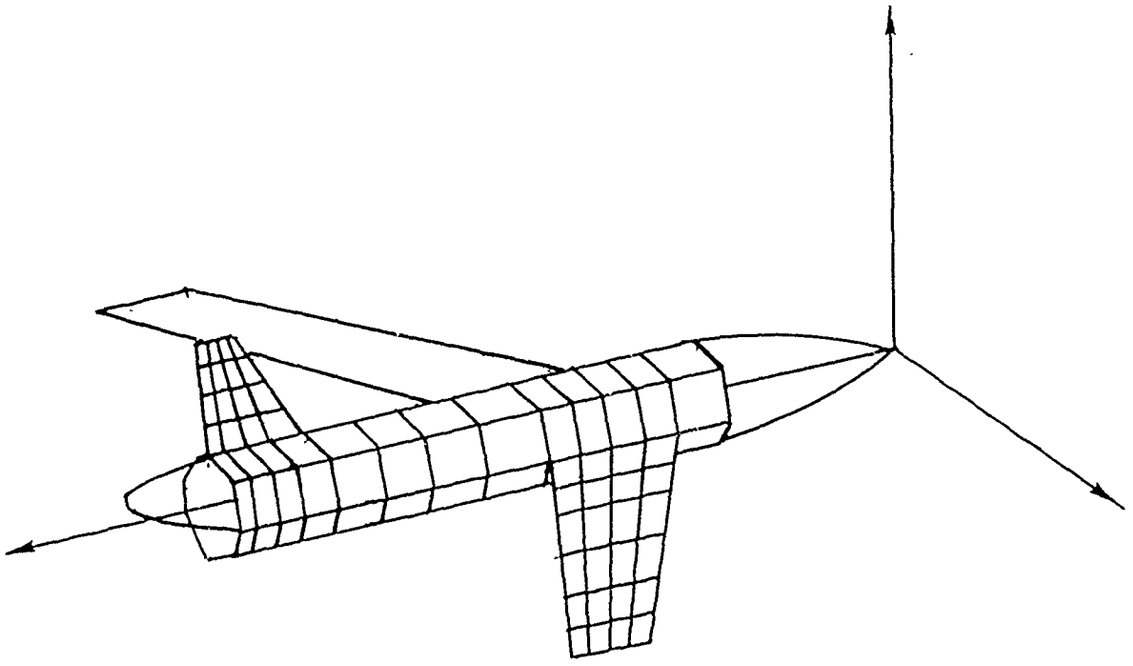

Sketch 2.2-2

The body, then, is made up of two separate components. (1) an axial pressure potential doublet distribution whose strength is obtained from slender body theory and (2) lifting surface elements placed on the body surface whose strength is obtained by a solution of equation (2.2-13).

2.3 The Normalwash Boundary Conditions

The normalwash boundary conditions for the lifting surface elements are determined by assuming the surfaces move normal to themselves with a displacement distribution given by h. These normal motions are given by a series of mode shapes, f_i and generalized coordinates $\bar{q}_i$

$$h = s \sum f_i \bar{q}_i \tag{2.3-1}$$

The normalwash boundary condition is given by the substantial derivative of h, i.e., Dh/Dt. The normalwash for mode i is:

$$\frac{W_i}{U_\infty} = w_i = \frac{df_i}{d(x/s)} + i \frac{\omega s}{U_\infty} f_i$$

$$= \frac{df_i}{d(x/s)} + i k_r \left(\frac{2s}{\bar{c}}\right) f_i \tag{2.3-2}$$

where $k_r = \dfrac{\omega \bar{c}}{2 U_\infty}$

The mode shapes may be input numerically (both f_i and $df_i/d(x/s)$ may be input) or as polynomials.

$$f_i = \text{coef} \sum_{n=0}^{5} \sum_{m=0}^{5} a_{inm} \left(\frac{x}{s}\right)^n \left(\frac{\tau}{s}\right)^m \tag{2.3-3}$$

Here τ is a lateral parameter representing the radial distance from the x-axis to a point on the surface or the radial distance from the inboard edge of a particular lifting surface panel to a point on the surface (see Input Procedure, Part I, Vol II). The constant coef is simply a scale factor.

The x-derivative of f_i is used in Equation (2.3-2) and is:

$$df/d(x/s) = \text{coef} \sum_{n=0}^{5} \sum_{m=0}^{5} n\, a_{inm} \left(\frac{x}{s}\right)^{n-1} \left(\frac{\tau}{s}\right)^{m} \qquad (2.3\text{-}4)$$

The upwash and sidewash to the bodies, i.e., $w^{(f)}$ are also determined from Equation (2.3-2) except that there are separate modes for the z and y-directions of motion.

The slender body theory of Miles requires the derivative of $w^{(f)}$

$$\frac{dw^{(f)}}{dx} = \frac{1}{s} \frac{dw_i^f}{d(x/s)} = \frac{1}{s} \left\{ \frac{d^2 f_i}{d^2(x/s)} + ik_r \left(\frac{2s}{\bar{c}}\right) \frac{df_i}{d(x/s)} \right\} \qquad (2.3\text{-}5)$$

where

$$\frac{d^2 f_i}{d^2(x/s)} = c \sum_{n=0}^{5} \sum_{m=0}^{5} n(n-1) \left(\frac{x}{s}\right)^{n-2} \left(\frac{\tau}{s}\right)^{m} \qquad (2.3\text{-}6)$$

If modes are input numerically (f_i and $df_i/d(x/s)$ then $d^2f_i/d^2(x/s)$ must be determined numerically. An alternate procedure may be suggested here. Instead of f_i and $df_i/d(x/s)$ the terms f_i and $d^2f_i/d(x/s)^2$ could be input. The term $df_i/d(x/s)$ is then obtained by numerical integration of $d^2f_i/d(x/s)^2$ which is more accurate than numerical differentiation*.

Also required for the slender body solution is dR_o/dx. This quantity may be obtained numerically from the input R_o. An alternate approach may again be suggested whereby dR_o/dx is input and R_o is obtained by numerical integration.

*Actually the first value of $df_i/d(x/s)$ is input along with the second derivatives to establish the proper level for $df_i/d(x/s)$.

2.4 Loads and Forces

2.4.1 Generalized Forces

The lifting pressures, ΔC_p, on the lifting surfaces are given by the solution of (2.2-13). The lifting pressures, $\Delta C_p^{(f)}$, on the bodies are given by (2.2-4). These two distributions may be combined into one partitioned array, $\overline{\Delta C}_p$ as follows:

$$\left\{ \overline{\Delta C}_p \right\} = \left\{ \begin{array}{c} \Delta C_p \\ \hline \Delta C_p^{(f)} \end{array} \right\} \qquad (2.4\text{-}1)$$

The lifting pressure $\Delta C_p^{(f)}$ is composed of two components, i.e., ΔC_Z and ΔC_Y.

$$\Delta C_p^{(f)} = \left\{ \begin{array}{c} \Delta C_Z \\ \hline \Delta C_Y \end{array} \right\}$$

The lifting pressure ΔC_Z acts on the area of the body projected onto the $z = 0$ plane. The lifting pressure ΔC_Y acts on the area of the body projected onto the $y = 0$ plane. All loadings are in the form of pressures acting on areas and the calculation of the generalized forces may proceed on this basis. There are as many lifting pressure distributions as there are modes. The subscript "i" identifying the mode will be added to ΔC_p.

$$\overline{\Delta C}_p = \sum_i \overline{\Delta C}_{p_i} \, \overline{q}_i$$

The generalized forces, Q_{ij}, associated with the generalized coordinates, $\overline{q}_i$, are determined using the principle of virtual work. The virtual work, δW_j associated with the j^{th} mode is:

$$\delta W_j = \int_{L.} \int_{S.} \overline{q} \cdot \overline{\Delta C}_{p_j} \, \delta h \, ds \qquad (2.4\text{-}2)$$

The same virtual work is obtained using the generalized forces

$$\delta W_j = -2\, s^3 q \sum Q_{ij}\ \delta\bar{q}_i \qquad (2.4\text{-}3)$$

Recalling, from (2.3-1), that

$$h = s \sum f_i\ \bar{q}_i$$

and equating (2.4-2) and (2.4-3) gives

$$-2\, s^2 q \sum Q_{ij}\ \delta\bar{q}_i = \sum sq \left\{ \int_{L.} \int_{S.} \overline{\Delta C}_{p_j}\ f_i\ ds \right\} \delta\bar{q}_i$$

Solving for Q_{ij} gives:

$$Q_{ij} = -\frac{1}{2s^2} \int_{L.} \int_{S.} \overline{\Delta C}_{pj}\ f_i\ ds \qquad (2.4\text{-}4)$$

Numerically, the double integral is replaced by a summation:

$$Q_{ij} = -\frac{1}{s^2} \sum_n \left\{ \overline{\Delta C}_{pj}\ f_i \right\}_n \Delta s_n \qquad (2.4\text{-}5)$$

where Δs_n is the box area on the lifting surfaces and where Δs_n is $R_o\, \Delta\xi_n$ on the projected body surfaces. The factor 1/2 is accounted for by restricting the range of the subscript "n" to the right-half of the aircraft. (Even the projected area of the body is halved, i.e., $\Delta s_n = R_o \Delta\xi_n$ if it lies on the plane of symmetry.)

2.4.2 Aerodynamic Parameters

It is desirable and sometimes necessary to generate conventional aerodynamic data. Such data, in addition to being useful in themselves,

provide an excellent check for the computer program and/or specific cases to be run by it. For example, a check of the span loading for rigid body pitching and/or plunging could bring to light some geometrical data error in a particular case. Thus the aerodynamic data output acts as a program monitor.

The local normal force coefficient and pitching moment coefficient about the local leading edge is

$$c_n = \frac{1}{c} \int \Delta C_p \, d\xi \tag{2.4-6}$$

$$c_m = \frac{-1}{c^2} \int \Delta C_p \, (\xi - x_{L.E.}) \, d\xi \tag{2.4-7}$$

where c is the local chord length. The total lift and side force coefficients are:

$$C_Z = \frac{(1+\delta)}{A} \left\{ \int_{R.S.} c \, c_n \, d\eta + g \int_{B.} R_o \, \Delta C_Z \, d\xi \right\} \tag{2.4-8}$$

$$C_Y = \frac{(1-\delta)}{A} \left\{ - \int_{R.S.} c \, c_n \, d\zeta + g \int_{B.} R_o \, \Delta C_Y \, d\xi \right\} \tag{2.4-9}$$

Here A is the reference area, δ is a symmetry flag ($\delta = 1$, for symmetry, $\delta = -1$, for antisymmetry and $\delta = 0$ for asymmetry). The limit, R.S., indicates that the integration is to be carried out over the right side of the aircraft and the limit B. indicates that the integrals are to be taken along the lengths of the bodies. The term g is defined in Eq. (2.4-12). The pitching moment, yawing moment and rolling moment coefficients are given by:

$$C_m = \frac{(1+\delta)}{A\bar{c}} \left\{ \int_{R.S.} (c^2 \, c_m - (x_{L.E.} - x_R) \, c \, c_n) \, d\eta \right. \tag{2.4-10}$$

$$\left. - g \int_{B.} \Delta C_Z \, (\xi - x_R) \, R_o \, d\xi \qquad (+ \text{ nose up}) \right\}$$

$$C_n = -\frac{(1-\delta)}{2As}\left\{\int_{R.S.}(c^2 c_m - (x_{L.E.} - x_R)\, c\, c_n)\, d\zeta + g\int_{B.}\Delta C_Y\,(\xi - x_R)\, R_o\, d\xi\right\} \qquad (2.4\text{-}11)$$

(+ nose right)

$$C_\ell = -\frac{(1-\delta)}{2As}\left\{\int_{R.S.} c\, c_n\, \eta\, d\eta + \int_{R.S.} c\, c_n\, \zeta\, d\zeta + \eta_a 2\int_{B.}\Delta C_Z\, R_o\, d\xi + \zeta_a 2\int_{B.}\Delta C_Y\, R_o\, d\xi\right\} \qquad (2.4\text{-}12)$$

(+clockwise, right wing down)

where $g = \begin{cases} 1 \text{ if } \eta_a = 0 \\ 2 \text{ if } \eta_a > 0 \end{cases}$

where x_R is the point about which moments are taken. The rolling moment is taken about the x-axis.

Dynamic stability derivatives can be obtained from the complex coefficients just described. Each complex aerodynamic coefficient possesses an in-phase and an out-of-phase component, the real part being the component in phase with the motion and the imaginary part the component out of phase with the motion (90° out of phase). Reference 11 describes a

method for determining dynamic stability derivatives. Specifically, if C represents any aerodynamic coefficient such as c_n, c_m, C_Z C_m etc., and if the subscripts α and θ represent modified plunging and pitching then:*

$$C_\alpha = C_\alpha \ (k_r = 0) \qquad \text{static derivative}$$

$$C_{\dot{\alpha}} = \frac{1}{k_r} \text{ Im } C_\alpha \ (k_r = \epsilon) \qquad \text{damping derivative}$$

$$C_{\ddot{\alpha}} = -\frac{1}{k_r^2} \text{ Re } \{ C_\alpha \ (k_r = 0) - C_\alpha \ (k_r = \epsilon) \} \qquad \text{acceleration derivative}$$

The program must be run at two different values of reduced frequency $k_r = 0$ and $k_r = \epsilon$ to obtain these dynamic derivatives. The value of ϵ is usually small (about 0.1). The dynamic derivatives will then be valid for aircraft motions in the frequency range 0 to ϵ.

The values of the q or pitch-rate derivatives are obtained as follows:

$$C_q = \frac{1}{k_r} \text{ Im } C_\theta \ (k_r - \epsilon) - C_{\dot{\alpha}}$$

$$C_{\dot{q}} = \frac{1}{k_r^2} \text{ Re } \{ C_\theta (k_r = 0) - C_\alpha \ (k_r = \epsilon) \} - C_{\ddot{\alpha}}$$

Similar expressions for C_β, $C_{\dot{\beta}}$, $C_{\ddot{\beta}}$, C_r and $C_{\dot{r}}$ are obtained if the values of C_α and C_θ are replaced by values for modified sideslipping and yawing. The expressions for the rolling damping and acceleration derivatives are obtained as follows:

$$C_p = C_p \ (k_r = 0)$$

$$C_{\dot{p}} = \frac{1}{k_r} \text{ Im } C_p \ (k_r = \epsilon)$$

where C_p is the complex aerodynamic coefficient due to unit rolling velocity.

* The term "modified" indicates that the amplitude of translation (plunging or sideslipping is normalized by the term (ik_r). The resulting derivatives, then, pertain to α and β respectively.

2.5 Aerodynamic Influence Coefficients and Harmonic Gust Coefficients

2.5.1 General Considerations

The aerodynamic influence coefficient matrix used in this method is described in References 12 and 13. The basic idea is to produce a set of influence coefficients that are independent of mode shape and smaller in number than the number of elements or boxes. An obvious set of AIC's would be $[D]^{-1}$ whereby lifting pressures are obtained directly from the normalwash boundary conditions. A second example would be the matrix of generalized forces $[Q]$, a typical element of which is Q_{ij}. The advantage of $[D]^{-1}$ is that it is independent of mode shape; the advantage of $[Q]$ is that it is small and easily handled. A compromise between $[D]^{-1}$ and $[Q]$ is the current [AIC]. A preselected set of "submodes" is selected for each lifting surface strip or bay. The submode allows motion only on the strip or bay considered. A set of generalized forces is obtained from each of these submodes. For instance if the submodes are pitching and plunging and there are 15 bays then the AIC will be a 30 x 30 matrix of generalized forces. It is assumed that the general mode shapes may be built up of these submodes by superposition. The generalized force matrix for any specific mode shape is then

$$Q_{ij} = \{ \bar{f}_j \}^T [AIC] \{ \bar{f}_i \}$$

where $\bar{f}_i$ are components of the i^{th} mode shape in terms of the submodes.

The value of using AIC's lies in the fact that once the matrices of AIC's have been generated for a specific planform, Mach number and reduced frequency, any number of aeroelastic analyses can be performed in which only the inertial and stiffness properties are altered, since the AIC's are independent of the aircraft vibration mode shapes and/or static deflection modes.

The aerodynamic influence coefficients, as derived in Reference 12, relate the oscillatory aerodynamic moments and/or forces acting at the specified AIC control points to the harmonic rotations and/or deflections of these control points. By the definition of Reference 12 the equation for the dimensional AIC matrix is

$$[C_h]_d = \frac{1}{2} \rho_o \frac{U_\infty}{b_r} (\bar{c}/2) [B] [D]^{-1} [W] \qquad (2.5\text{-}1)$$

where $\bar{c}/2$ is the reference semi-chord, $\frac{U_\infty}{b_r \omega}$ is the reference reduced velocity, [B] is the integration matrix described in Sec. 2.5-3, and [W] is the substantial derivative matrix described in Sec. 2.5-2.

A set of dimensional static AIC's $[C_{hs}]_d$ may also be defined by

$$[C_{hs}]_d = \frac{1}{2} \rho_o (\bar{c}/2) [B] [D\ (k_r = 0)]^{-1} [W] \qquad (2.5\text{-}2)$$

These can be used in static aeroelastic analyses of lift effectiveness, divergence, control surface effectiveness, reversal, and so forth.

The harmonic gust coefficients were also derived in Reference 12 for a gust in the plane of the surface. For a gust field in a plane with arbitrary dihedral* Γ_g, Eq. (39) of Reference 12 is generalized to read

$$\{G\} = \frac{1}{2} \rho_o U_\infty W_g [B] [D]^{-1} \left\{ \cos(\Gamma_g - \gamma) \exp\left(-ik_r \frac{(x-x_o)}{c/2}\right) \right\} \qquad (2.5\text{-}3)$$

where U_∞ is the aircraft velocity, W_g is the harmonic gust amplitude, k_r is the reduced frequency, γ is the local surface dihedral, and x_o is the gust reference coordinate.

* Vertical velocities are obtained when the dihedral angle is zero. If the dihedral angle is -90° the gust velocities are in the lateral (+y) direction.

2.5.2 The Substantial Derivative Matrix

The Doublet-Lattice Method requires the determination of the oscillatory normalwash on the lifting surface at the 3/4-chord of each box In the derivation of the substantial derivative matrix, [W], we assume that the aerodynamic idealization for the particular aeroelastic problem provides a sufficient number of (spanwise) strips on the lifting surface so that the oscillatory normalwash on each box can be determined only by chordwise interpolation and differentiation of the assumed local deflection mode shapes corresponding to each local aerodynamic degree of freedom. It is assumed that an interpolation matrix, $[W_I]$, can be found such that

$$\{ h_{3c/4} \} = [W_I] \{ h \}$$

where $h_{3c/4}$ denotes the deflection at the 3/4-chord point of each box and h denotes the AIC control point deflections. The matrix $[W_I]$ has the partitioned form

$$\begin{Bmatrix} h^{(1)}_{3c/4} \\ h^{(2)}_{3c/4} \\ \cdot \\ \cdot \\ \cdot \\ h^{(n)}_{3c/4} \end{Bmatrix} = \left[\begin{array}{c|c|c|c} W_I^{(1)} & 0 & & 0 \\ \hline 0 & W_I^{(2)} & & 0 \\ \hline & & \ddots & \\ \hline 0 & 0 & & W_I^{(n)} \end{array}\right] \begin{Bmatrix} h^{(1)} \\ h^{(2)} \\ \cdot \\ \cdot \\ \cdot \\ h^{(n)} \end{Bmatrix} \qquad (2.5\text{-}1)$$

where the superscripts indicate strips in the aerodynamic idealization of the lifting surface. The oscillatory normalwash at the 3/4-chord of each box is given by

$$\frac{w(x)}{U_\infty} = \frac{dh(x)}{dx} + i \frac{k_r}{\bar{c}/2} h(x) \qquad (2.5\text{-}5)$$

Generalizing Eq. (2.5-5) in matrix notation we have

$$\{\bar{w}\} = [W]\{h\} \qquad (2.5\text{-}6)$$

where

$$[W] = \left[\frac{dW_I}{dx}\right] + i \frac{k_r}{\bar{c}/2} [W_I] \qquad (2.5\text{-}7)$$

Several alternatives to the computation of the [W] matrix can be used depending on the manner in which the deflection characteristics of the aircraft are described. Ref. 12 describes three possible alternatives for the [W] matrix; Alternative No. 1 is used in the generation of the AIC's for planar surfaces by computer program H7WA. The nonplanar computer programs, H7WB and H7WC have the capability of generating AIC's for nonplanar surfaces according to either of the two alternatives of the [W] matrix described in Reference 13 in Appendices I and II, which are reproduced in Appendix D.

The two alternatives describe two types of submodes that can be used. The submodes for each bay are:

1) Alternative #1: plunging, pitching, control surface rotation and tab rotation or control surface plunging.

2) Alternative #2. Three cambering modes, control surface rotation, or tab rotation.

Alternative #1 makes available six degrees of freedom or submodes per bay, while Alternative #2 furnishes seven. Of these available degrees of freedom or submodes only four may be used at one time. The reason

for this restriction is the limited core capacity of the computer. More of these available submodes may be made available if a core larger than 32K is available.

2.5.3 The Integration Matrix

The integration matrix, [B], relates the pressures over the lifting surface to the AIC control point moments and/or forces (Ref. 12)

$$\{ F \}_{AIC} = q[B] \{\Delta C_p\} \qquad (2\ 5\text{-}8)$$

where q is the dynamic pressure. It is assumed that there is a chordwise interpolation matrix, [Z], on each strip such that

$$h_{c/4} = [Z]\{h\} \qquad (2\ 5\text{-}9)$$

where the $h_{c/4}$ are the deflections at the 1/4-chord of each box and h are again the AIC control point deflections. [Z] has the same partitioned form as the matrix $[W_I]$ (Eq. 2.5-4).

$$\begin{Bmatrix} h_{c/4}^{(1)} \\ h_{c/4}^{(2)} \\ \cdot \\ \cdot \\ \cdot \\ h_{c/4}^{(n)} \end{Bmatrix} = \begin{bmatrix} Z^{(1)} & 0 & & 0 \\ 0 & Z^{(2)} & & 0 \\ & & \ddots & \\ 0 & & & Z^{(n)} \end{bmatrix} \begin{Bmatrix} h^{(1)} \\ h^{(2)} \\ \cdot \\ \cdot \\ \cdot \\ h^{(n)} \end{Bmatrix}$$

The generalized forces acting at the 1/4-chord of each box are given by

$$\{ F_{c/4} \} = q \lceil A \rfloor \{ \Delta C_p \} \qquad (2.5\text{-}10)$$

where $\lceil A \rfloor$ is the diagonal matrix of box areas. By applying the principle of virtual work it is seen that

$$\{ F \}_{AIC} = [Z]^T \{ F_{c/4} \} \qquad (2.5\text{-}11)$$

By combining Eqs. (2.5-10) and (2.5-11) and comparing with Eq. (2.5-8) we have

$$[B] = [Z]^T \lceil A \rfloor \qquad (2.5\text{-}12)$$

The actual form of the [B] matrix depends on the manner in which the deflection characteristics of the aircraft are described, and hence, on the form of the [W] matrix. The two alternatives for the [B] matrix are described in Reference 12 along with the corresponding [W] matrix forms.

2.6 Matrix Solution

When modes are considered the matrix equation (2.2-13) must be solved for each mode. The symbolic solution for multiple modes is

$$[\Delta C_p] = [D]^{-1} [w - w_B] \tag{2.6-1}$$

where the matrices $[w - w_B]$ and $[\Delta C_p]$ are the normalwash and resulting pressures for all of the modes. Each column of either $[\Delta C_p]$ or $[w - w_B]$ represents one mode. For AIC's Equation (2.5-1) must be solved

$$[C_h]_d = \frac{1}{2} \rho_o \frac{1}{k_r} (\bar{c}/2) [B] [D]^{-1} [W] \tag{2.6-2}$$

In both cases the symbolic solution contains a term like $[D]^{-1} [wr]$ where $[wr]$ is $[w - w_B]$ in (2.6-1) and $[W]$ in (2.6-2). Define the term $[D]^{-1} [wr]$ as $[P]$.

$$[P] = [D]^{-1} [wr] \tag{2.6-3}$$

In the present method the desired solution matrix $[P]$ is not obtained exactly as shown in this equation. The inverse, in the usual sense of the word, is not determined since this would be very inefficient for large matrices

The solution matrix $[P]$ is obtained directly from the equation

$$[wr] = [D] [P] \tag{2.6-4}$$

by direct Gaussian Triangularization and back solution. This subroutine is called SOLVIT and is described in Reference 14. The disadvantage of this procedure is that future solutions can be obtained only by a repetition of the triangularization and back solution (a $(1/3)N^3 + N^2 M$ process), where N is the order of the matrix $[D]$ and M is the order of $[wr]$). Also the solution matrix $[P]$ must fit into the computer core. When $[P]$ is small, as with the

modal approach, this restriction is not important. However for AIC's the solution matrix may be larger than the available storage.

A generalization of this method may be made to eliminate both disadvantages discussed above (see Reference 14, page 37). The basic idea is to save the instructions needed to triangularize the matrix [D]. It just so happens that these instructions come in the form of constants, the number of which fit into the empty space generated in [D]. by triangularization. The triangularized form of [D] fits into the upper triangular sector, including the diagonal, while the constants of triangularization fit into the lower triangular sector, excluding the diagonal. This matrix is termed the Quasi-Inverse since both halves of the matrix can be used to find a solution using only N^2 operations per mode or submode. The Quasi-Inverse requires identically the same number of operations as a direct solution, i. e., $(1/3)N^3$ operations. In fact this modified form of SOLVIT works exactly like SOLVIT if the solution matrix fits in core (except that the Quasi-Inverse matrix must be read on tape as it is generated so that it can be used in the future.)

The difficulty of running future solutions is thus solved Future solutions are solved simply by calling back the Quasi-Inverse and performing an N^2M operation (where M is the number of modes or submodes).

The restrictive requirement that the solution matrix fit into core is also eliminated since the normalwash matrix may be split into, say, two or more parts, each of which fit into the computer core. The first part of the solution corresponding to the first part of the normalized matrix obtained during the first pass through the computer ($(1/3)N^3 + N^2M$ operations). Also formed during this pass is the Quasi-Inverse. The second and subsequent passes through the computer generate the remainder of the solution (MN^2 operations each). The second and remaining parts are thus considered future solutions. This method is programmed in two parts QUAS and FUTSOL QUAS forms the Quasi-Inverse and solves for the first part of the solution and FUTSOL generates future solutions from the Quasi-Inverse.

3.0 CALCULATED RESULTS

3.1 Convergence of Results

The number of boxes necessary to give a converged result is dependent on the reduced frequency. For the steady case the convergence is very rapid. In fact, one box chordwise gives usable results (the method of Weissinger uses one box per spanwise station).

For the other extreme, many boxes are necessary for very high reduced frequencies. As an example, Figure 1 presents a convergence study for a reduced frequency (based on the span 2s, $k_r = \frac{\omega 2s}{2V_\infty}$) of 1.5. As shown in the figure the wave length corresponding to this frequency is approximately the length of the wing-tail assembly. This means that the effect of the wing on the tail is out of phase with the wing motion about 180°. Thus the downwash of the wing on the tail is opposite to the wing motion. This is a very severe case and many chordwise boxes are required. The figure shows that approximately 25 boxes per wave length are required. Thus for this case the box length ΔX_s is related to the reduced frequency by:

$$\frac{\Delta X_s}{\bar{c}} \leq \frac{\pi}{25 k_r} \text{ where } k_r = \frac{\omega \bar{c}}{2V_\infty}$$

Actually the wing and tail box lengths are not equal for Figure 1. The number of chordwise boxes for wing and tail are:

TOTAL	WING	TAIL
9	5	4
11	6	5
14	8	6
18	10	8
22	12	10

There are twelve spanwise strips for the case presented in Figure 1. A case using eight spanwise strips is also shown for the case of 22 total chordwise elements. The error for the real and imaginary parts is about 2.5% and 0.80%, respectively.

3.2 Nearly Coplanar Wing-Tail Configurations

The difficulty encountered by the Doublet-Lattice Method of Reference 1 for nearly coplanar wing-tail combinations is discussed in Section 2.1. The refinement of the method is also presented there. Figure 2 presents results for a nearly coplanar wing-tail configuration using both the original (unrefined) and the refined methods.

The wing-tail assembly is made to plunge with a reduced frequency of 0.6 (based on a chord length of 0.87424 s). The total lift coefficient (wing plus tail) is given (based on total area of both surfaces). It can be seen that the original method starts to lose accuracy when the gap to chord ratio is about 0.1. (Notice that the widths of the first eight strips is 0.1). The refined Doublet-Lattice Method gives accurate results for small $z/\bar{c}$. Appendix B explains that a numerical limit must be taken in the new or refined method. Any inaccuracies generated from this limit are not apparent even at a value of $z/\bar{c}$ of 0.025. Thus the refined method is valid for all practical cases of interest.

The wing-tail configuration of Figure 1 is used to present a second "gap" study (see Figure 3). A much wider range of vertical separation (gap) between the wing and tail is used.* Also the reduced frequency is considerably higher. Again the assembly is made to plunge and the total lift coefficient (based on the area of the wing alone) is given versus vertical spacing or "gap". Although not entirely evident the curves of real and imaginary parts of the lift coefficient have horizontal tangents as $z \to 0$ since they are symmetrical with z.

3.3 Wing-Body Combinations

The methods of Woodward (Ref. 6) and Giesing (Ref. 3) handle wing-body combinations in steady flow. A recent unpublished extension of Reference 3 allows bodies of varying diameter to be handled. These methods can be used to furnish test cases for the present method, at least for the static case.

---

* The tail moves aft as it moves up along the line $x = 0.875z$.

Figure 4 presents the span loading ($cc_\ell/\bar{c}$) for a wing-fuselage combination as calculated by the present method and the methods of Woodward (Ref. 6) and Giesing (modified Ref. 3). The configuration shown in the figure consists of a low aspect ratio wing attached at midplane to a thick parabolic body of revolution. The center of the wing root is at the center of the fuselage. The maximum diameter is 1/3 the span. The constant section, upon which lifting surface elements are placed, is half the length of the body and centered longitudinally. The span loadings shown in Figure 4 are entirely fuselage induced since the wing is held at zero incidence. In Figure 4(a) the fuselage is given an angle of attack of 1.0 radian. It can be seen that the present method agrees almost exactly with the method of Woodward* since the idealization for these two methods is about the same. The disagreement with the method of images (modified version of Ref. 3) is due to the fact that a different idealization is used. The boundary condition on the fuselage surface is satisfied using a system of images, one for each horseshoe vortex, plus an axial singularity system.

The span loading across the fuselage is induced by the wing loading (which was induced by the body incidence or camber) This loading is the fuselage lift carry-through. Slender body theory predicts no net load since the body closes.

Figure 4(b) shows the span load on the wing when the fuselage possesses a parabolic camber with a maximum deflection equal to the maximum radius. The agreement between the present method and Woodward's method is almost exact.

Figure 5 presents a comparison of calculated spanwise load distribution obtained using three slightly different approaches to the interference problem. The configuration and flow condition used is that of Figure 4(a). The circles represent the present method and are the same as those in Figure 4(a). The squares represent a method that differs only slightly from the present method. The subtle difference between the two methods is that the flow field due to the body axial singularities is calculated

* The control point must be placed at 85% of the box to render Woodward's results correct. See Reference 5.

on all lifting surface panels, including the body panels, and not just on the wing panel as in the present method. Since the body panels do not lie exactly on the body surface, the total normalwash there is different from zero (since the axial singularities were meant to cancel the normal flow only at the exact location of the body surface). This slight difference is enough to cause large differences in the spanwise loading on the body surface even though the loading on the wing compares favorably with the present method.

A second alternative (method of Reference 5) is to use body panels alone to simulate the body surface. For this method no axial singularities are used. When the body possesses no angle of attack (boundary condition of zero normalwash to the body surface) the results are accurate (see Reference 5, Figure 12). However, when the body possesses an angle of attack or camber, then the results seem to be very inaccurate especially over the body surface. Figure 5 shows such a calculation. The reason for this inaccuracy at angle of attack is that the body panels are simulating an annular or ring wing. Such an annular wing is much more effective in lift than the body it represents. If the body has no region of separation and if no vortices are shed from the body then the only lift it can carry is the lift carry-through which is induced by the wings. The spanwise distribution of lift carry-through has the characteristic shape shown on Figures 4(a) and 4(b) The lift, over and above the lift carry-through, is caused by the annular wing effect of the body elements. A possible solution to this problem would be to use wakeless elements on the body surface. Such wakeless elements can be generated using two steady or unsteady horseshoe vortices: one placed behind the other such that the wakes cancel out.

Figure 6 presents an example of an unsteady wing-fuselage calculation. The configuration used is that of Figure 4. The two modes of oscillation are again the same as those used in Figure 4, for the static case. Specifically:

Mode 1 (Figure 6(a)) $\quad z = (x - x_c)\, e^{i\omega t}$

Mode 2 (Figure 6(b)) $\quad z = 4.0\, R_{max} \left(\frac{x - x_c}{L}\right)^2 e^{i\omega t}$

Here x_c, L and R_{max} are the center, length and maximum radius of the body respectively. The frequency of oscillation (based on the average chord, $\bar{c} = 7$) is $k_r = \frac{\omega \bar{c}}{2V} = 1.0$. The wing remains stationary while only the body is in motion. The span loading across the wing is induced by the body motions while the span loading across the body is induced by the loading on the wing. The span loading across the fuselage does not include the unsteady slender body component* and is just the lift carry-through.

A second wing-body case is presented in Figures 7, 8, and 9. The specific configuration considered, which is shown in Figure 7, is a wing with an engine nacelle mounted at its tip. The wing nacelle combination is made to plunge and pitch harmonically with a reduced frequency, (based on the semispan), of 1.72. The pitch axis is shown in Figure 7. The real and imaginary parts of the distribution of lift coefficient are given for both pitching and plunging. In addition, the distribution of lift coefficient for the wing alone is presented for reference. Notice that the nacelle has a substantial effect on the distribution of lift coefficient. This effect arises from two sources; the first is the upwash generated by the motion of the nacelle while the second is the end-plate effect of the nacelle or the wing tip.

The slender body simulation of the nacelle is accomplished using two bodies. The axes of the bodies are centered within the nacelle spanwise and given a vertical displacement of ± 0.108252. The radius of these bodies is 0.108252. Even though these two bodies do not quite fill up the nacelle cross-sectional area, it can be shown that this choice of center and radius gives the best representation of the flow around the nacelle cross-section (in two-dimensions).

Figures 8 and 9 present comparisons of experimental and calculated lifting pressure coefficient. Specifically, Figure 8 gives the pressure at two spanwise stations, $y/s = 0.27$ and 0.715 for the plunging case. The wing-

* Unsteady slender body theory gives a non-zero lifting force on a body even if a closed body is considered.

alone pressure distribution is also given at the spanwise station closest to the nacelle; i.e., y/s = 0.715.

Figure 9 gives the pressures at the same two stations for the pitching case. The test and theory correlate best at station y/s = 0.27 for both the pitch and plunge case. This may be due to flow separation on the aft portion of the wing which seems to be present in the vicinity of y/s = 0.716. The loss of lift aft of about the 80% chord point indicates that this is the case.

3.4 Conclusions

(1) The Doublet-Lattice Method is a simple, versatile and accurate lifting surface theory. The method is capable of analyzing lifting surfaces with arbitrary planform and dihedral. Control surfaces, either full- or partial-span, may be included. Problems of intersecting and/or interfering nonplanar configurations, such as a wing-pylon combination, a T- or V-tail, a wing-tail combination, etc., may be analyzed. The method documented here is also capable of solving problems involving lifting surfaces and bodies where the bodies may be in motion. Included in the calculations are options for

(a) Aerodynamic data including lifting pressures, spanwise lift and moment distributions, aerodynamic center locations, total lift and side force coefficients, and total pitching, yawing and rolling moments;

(b) Generalized forces for polynomial modes of motion specified by the user;

(c) Aerodynamic Influence Coefficients;

(d) Gust loads from a harmonic gust field;

(e) Symmetry and ground effects.

(2) A refined version of the original Doublet-Lattice Method is required for nearly coplanar wing-tail combinations The refinement consists of considering the planar and non-planar parts of the kernel separately. The details are given in Appendix B. As a control point approaches the plane of the sending element a limit is taken numerically This limiting procedure is accurate for all practical values of vertical displacement.

(3) The number of chordwise boxes must increase in proportion to the frequency; specifically, $\Delta x_s/\bar{c} \leq \pi/25k_r$ Other requirements exist for the placement of strips and boxes These requirements are discussed in Part I, Vol II.

(4) The boundary condition on the lifting surface elements, placed on body surfaces for wing-body interference purposes, must be zero normalwash. The elements on the body surface represent a ring or annular wing*. This annular wing must be used for interference purposes only; any angle of attack will produce an undesirable annular wing lift. A slender body theory for circular bodies is used to reduce the normalwash, generated by a body in motion, to zero.

(5) The tube on which lifting surface elements are placed, to generate wing-body interference, must have a constant cross-section along its length. The cross-sectional shape may be noncircular. The reason for this is that each element has a wake trailing straight back downstream to infinity If the tube were of varying radius, element wakes would be threading in and out of the body surface. Such an idealization has not been tried and its validity has not been proven.

The synthesis of a noncircular slender body theory out of one for circular bodies is accomplished by placing more than one circular body in close proximity. The distance

* Actually, the body cross-section may be of arbitrary shape even though the slender body theory is for a circular cross-section. A slender body theory for cross-sections of different shape could replace this simple theory.

between axes and the radius of the various bodies may be obtained from a two-dimensional analysis. This approach, although only approximate, is reasonably accurate. In general, the interference generated by the body elements is less than it should be by a small amount. Convergence studies have shown that as the number of elements on the body surface is increased the results tend toward those obtained using the image method

(6) The inverse of the normalwash factor matrix [D] need not be found to obtain a solution. Direct solution by triangularization is always preferable If the same problem is to be solved repeatedly, a method for saving the triangularization instructions (these are numbers which may be saved in the lower half of the triangularized [D] matrix) is used.

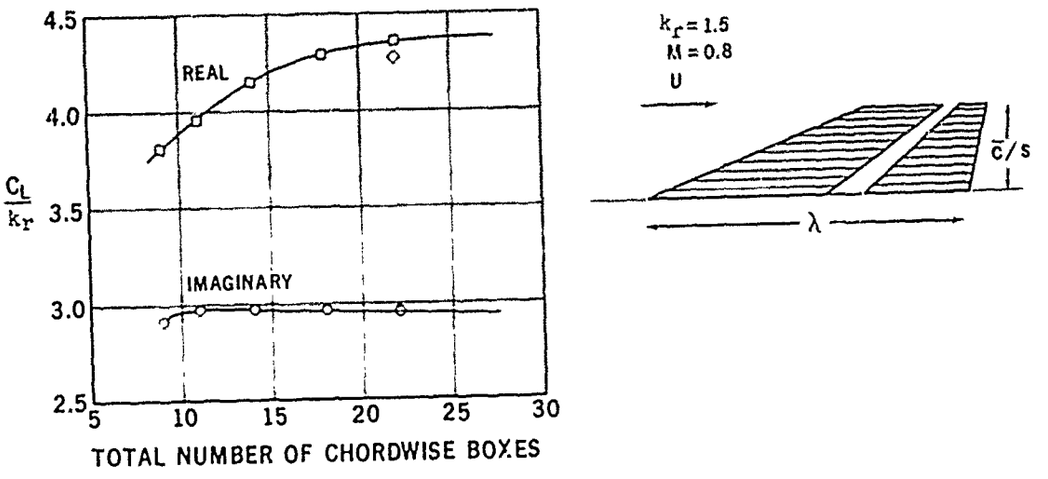

Figure 1. Variation of the Total Lift Coefficient with Box Number for a Wing Tail Combination Oscillating in Plunge.

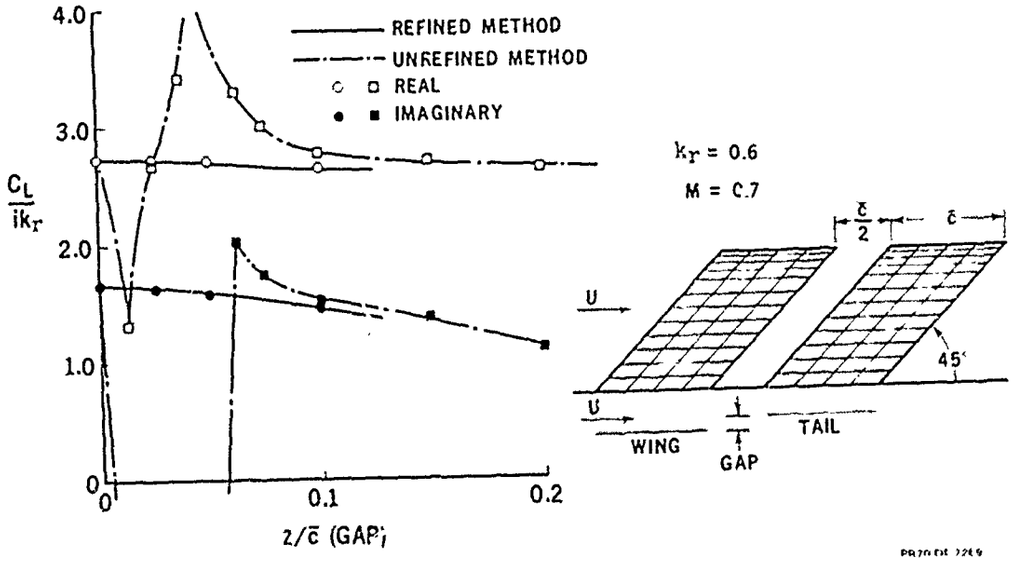

Figure 2. Variation of the Total Lift Coefficient with the Vertical Distance Between Wing and Tail for Plunging Motion.

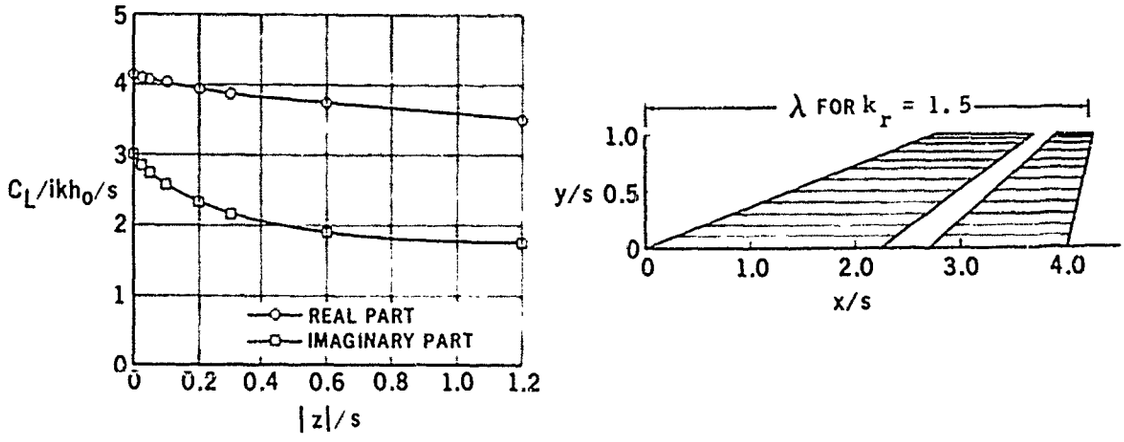

Figure 3. Variation of the Total Lift Coefficient with the Vertical Distance Between Wing and Tail for Plunging Motion.

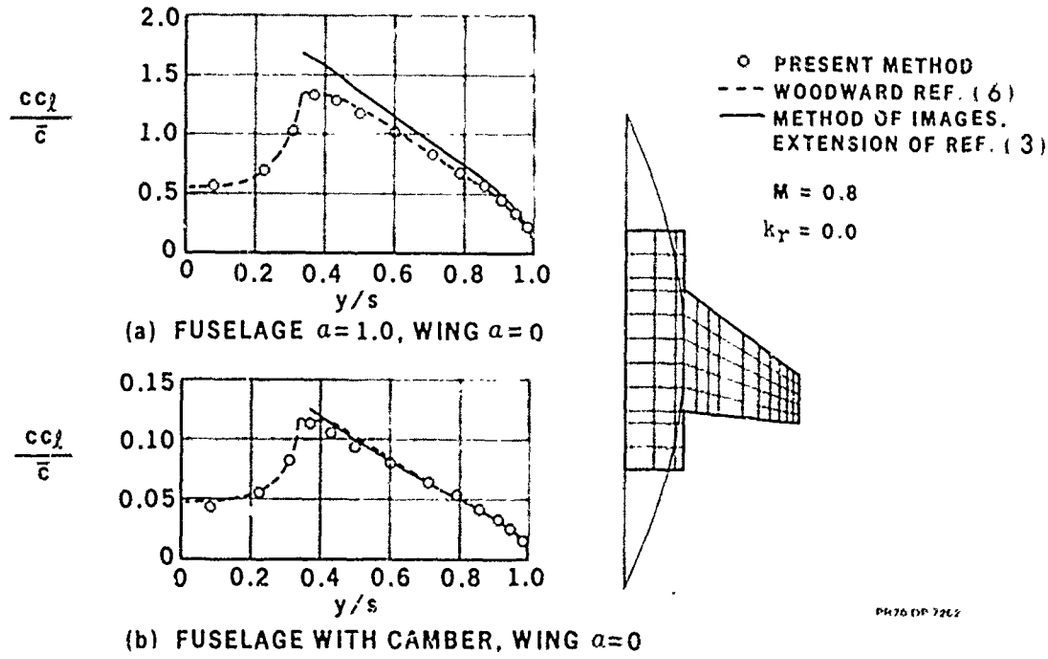

Figure 4. Span Load Distribution for a Wing-Body Combination in Steady Flow: (a) Body Angle of Attack = 1.0 Radian, Wing Angle of Attack = 0.0; (b) Body with Parabolic Camber, Wing at Zero Incidence.

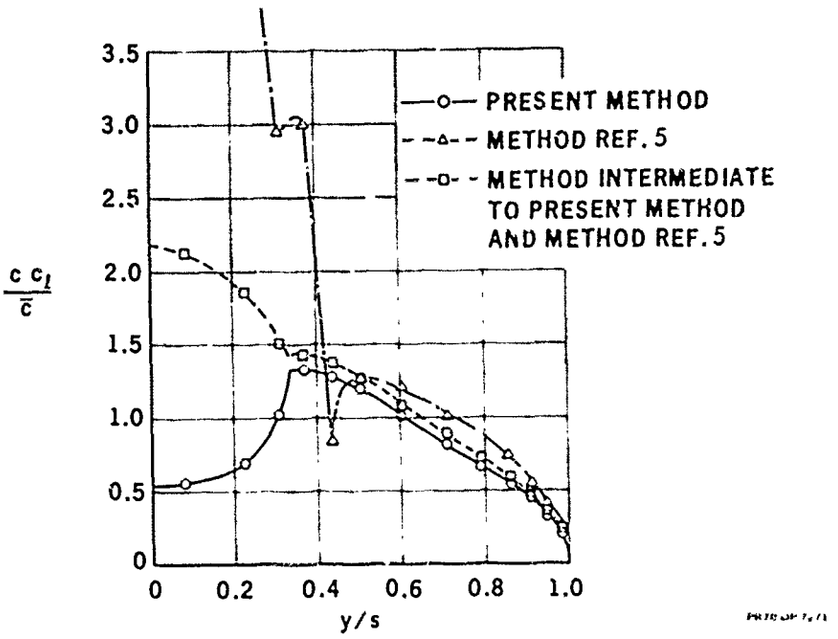

Figure 5. Span Load Distribution as Calculated by Three Different Methods.

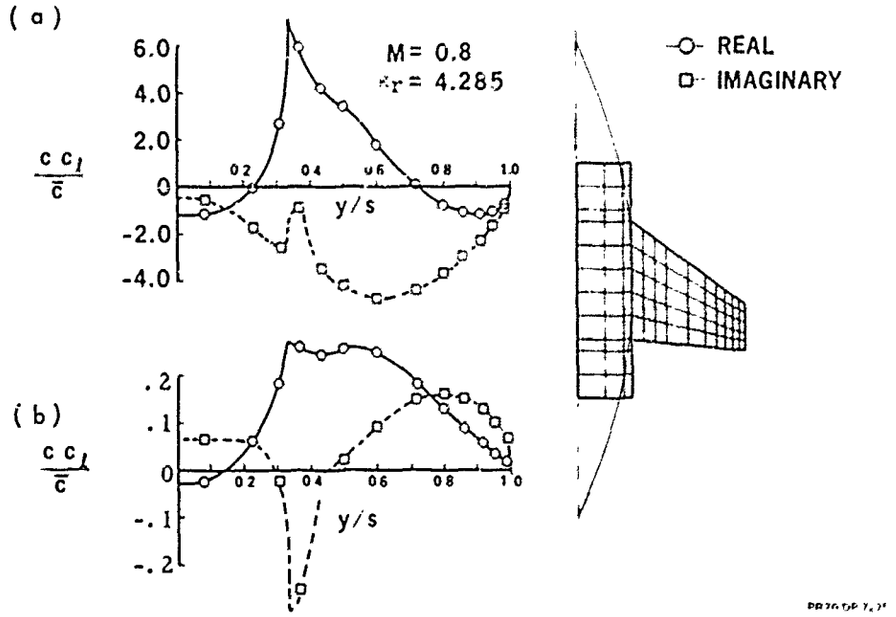

Figure 6. Span Load Distribution for a Wing-Body Combination in Unsteady Flow: (a) Body Pitching, Wing Stationary; (b) Body Cambering, Wing Stationary.

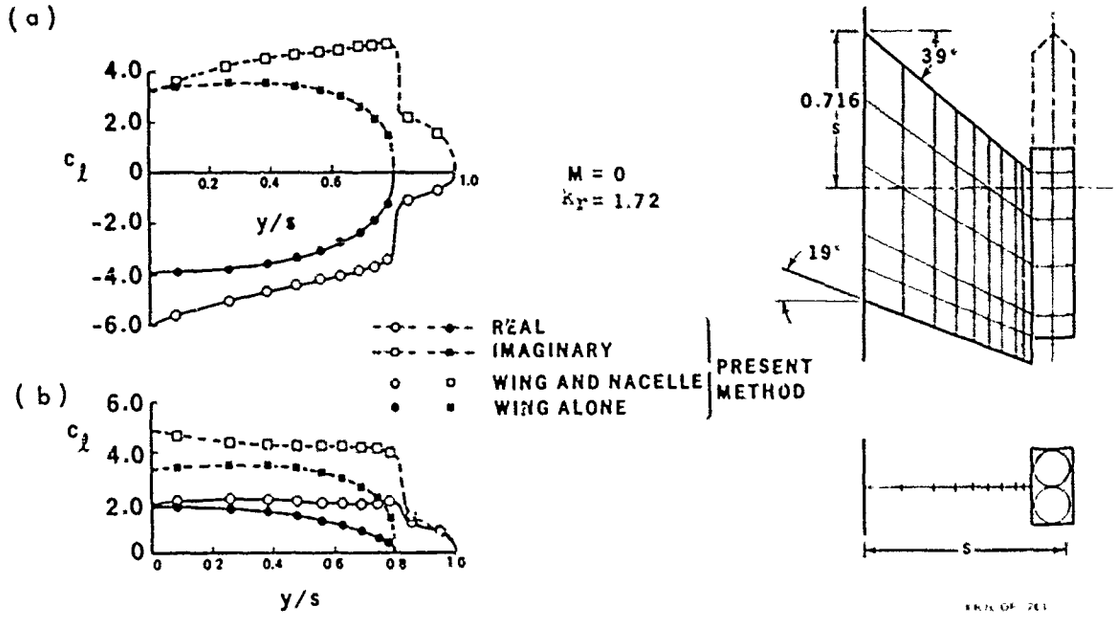

Figure 7. Distribution of Lift Coefficient for a Wing-Nacelle Combination (a) Plunging; (b) Pitching.

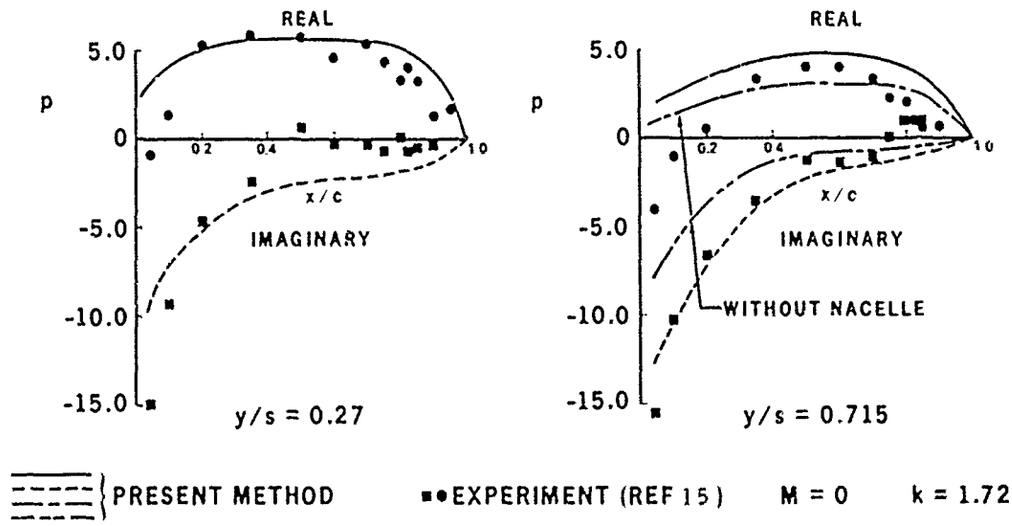

Figure 8. Comparison of Experimental and Calculated Lifting Pressure Coefficient for a Wing-Nacelle Combination in Plunge.

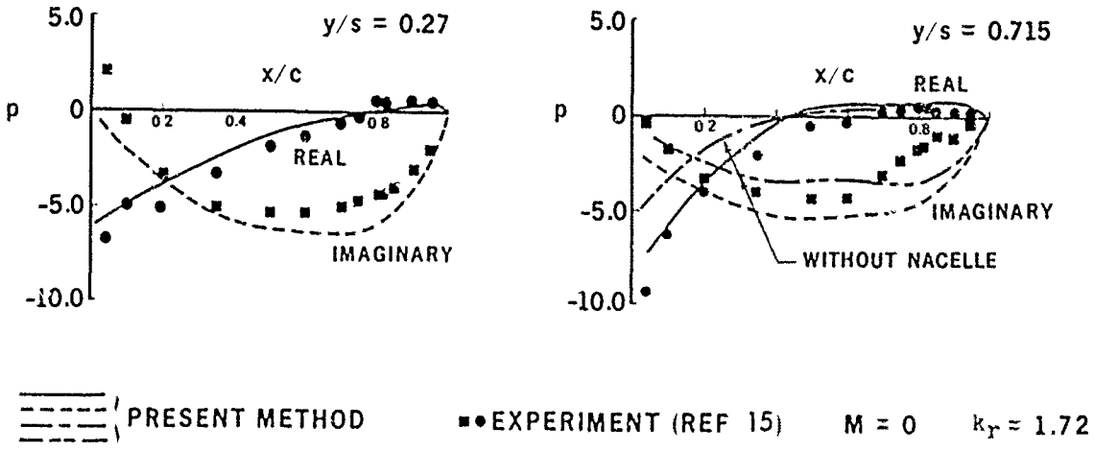

Figure 9. Comparison of Experimental and Calculated Lifting Pressure Coefficient for a Wing-Nacelle Combination in Pitch.

REFERENCES

1. Albano, E., and Rodden, W. P., "A Doublet-Lattice Method for Calculating Lift Distributions on Oscillating Surfaces in Subsonic Flows," AIAA J., Vol. 7, No. 2, Feb. 1969, pp. 279-285; errata, AIAA J., Vol. 7, No. 11, Nov. 1969, p. 2192.

2. Hedman, S. G., "Vortex Lattice Method for Calculation of Quasi Steady State Loadings on Thin Elastic Wings," Report 105, Oct. 1965, Aeronautical Research Institute of Sweden.

3. Giesing, J. P., "Lifting Surface Theory for Wing-Fuselage Combinations," Report DAC-67212, Aug. 1968, Douglas Aircraft Co.

4. James, R. M., "On the Remarkable Accuracy of the Vortex Lattice Discretization in Thin Wing Theory," Report DAC-67211, Feb. 1969, McDonnell Douglas Corp., Long Beach, California.

5. Kalman, T. P., Rodden, W. P., and Giesing, J. P., "Application of the Doublet-Lattice Method to Nonplanar Configurations in Subsonic Flow," Paper No. 70-539, presented to the AIAA Atmospheric Flight Mechanics Conf., 13-15 May 1970, Tullahoma, Tennessee. To be published in Journal of Aircraft.

6. Woodward, F. A., "Analysis and Design of Wing-Body Combinations at Subsonic and Supersonic Speeds," Journal of Aircraft, Vol. 5, No. 6, Nov.-Dec. 1968, pp. 528-534.

7. Vivian, H. T. and Andrew, L. V., "Unsteady Aerodynamics for Advanced Configurations. Part I - Application of the Subsonic Kernel Function to Nonplanar Lifting Surfaces," FDL-TDR-64-152, May 1965, Air Force Flight Dynamics Lab., Wright-Patterson Air Force Base, Ohio.

8. Landahl, M. T., "Kernel Function for Nonplanar Oscillating Surfaces in a Subsonic Flow," AIAA J., Vol. 5, No. 5, May 1967, pp. 1045-1046.

9. Miles, J. W., "On Non-Steady Motion of Slender Bodies," Aeronautical Quarterly, Vol. II, Nov. 1950, pp. 183-194.

10. Berman, J. H., Shyprykevich, P., and Smedfjeld, J. B., "A Subsonic Nonplanar Kernel Function for Surfaces Inclined to the Freestream," Journal of Aircraft, Vol. 7, No. 2, Mar.-Apr. 1970, pp. 188-190.

11. Rodden, W. P., and Giesing, J. P., "Application of Oscillatory Aerodynamic Theory to Estimation of Dynamic Stability Derivatives," Journal of Aircraft, Vol. 7, No. 3, May-June, 1970.

12. Stahl, B., Kalman, T. P., Giesing, J. P., and Rodden, W. P., "Aerodynamic Influence Coefficients for Oscillating Planar Lifting Surfaces by the Doublet Lattice Method for Subsonic Flows Including Quasi-Steady Fuselage Interference," Report DAC-67201, Oct. 1968, McDonnell Douglas Corp., Long Beach, California.

13. Kalman, T. P., Rodden, W. P., and Giesing, J. P., "Aerodynamic Influence Coefficients by the Doublet Lattice Method for Interfering Nonplanar Lifting Surfaces Oscillating in a Subsonic Flow," DAC-67977, Nov. 1969, Douglas Aircraft Co.

14. Hess, J. L., and Riddell, T. M., "Direct Solution of a Square Matrix Whose Size Greatly Exceeds High-Speed Storage," Douglas Aircraft Company Report DAC-70000, July 1969.

15. Laschka, B., "The Pressure, Lift and Moment Distributions on a Harmonically Oscillating Sweptback Wing of Low Aspect Ratio at Low Subsonic Speeds; Comparison Between Theory and Measurements," Proc. of International Council of the Aeronautical Sciences, Fourth Congress, 1964, Paris, pp. 295-313; translated in Royal Aircraft Establishment Library Translation 1223, April 1967.

16. Watkins, C. E., Runyan, H. L., and Woolston, D. S., "On the Kernel Function of the Integral Equation Relating the Lift and Downwash Distributions of Oscillating Finite Wings in Subsonic Flow," Report 1234, 1955, NACA.

17. Mangler, K. W., "Improper Integrals in Theoretical Aerodynamics," Report Aero 2424, C. P. No. 94, June 1951, Royal Aircraft Establishment.

18. Laschka, B., "Zur Theorie der harmonisch schwingenden tragenden Fläche bei Unterschallanströmung," Zeitschrift für Flugwissenschaften, Vol. 11, No. 7, July 1963, pp. 265-292.

APPENDIX A. THE KERNEL FUNCTION FOR LIFTING SURFACES

The velocity normal to an oscillating surface, $W = U_\infty \mathrm{Re}(\bar{w}e^{i\omega t})$, is related to the pressure difference, $P = q\,\mathrm{Re}(\Delta C_p e^{i\omega t})$, across the surface by the integral equation (Ref. 16)

$$\bar{w}(x_r, y_r, z_r) = \frac{1}{8\pi} \oint\!\!\!\!\!\!\int K(x_0, y_0, z_0; \omega, M)\Delta C_{p_s}(\xi, \eta, \zeta)d\xi\, d\sigma \qquad (A.1)$$

where x or ξ is the streamwise coordinate and σ is the tangential coordinate on the surface (see Figure A-1), ω is the frequency of oscillation, M is the Mach number, and subscript r denotes the downwash or receiving point and the subscript s denotes the doublet or the sending point, and

$$x_0 = x - \xi \qquad (A.2)$$

$$y_0 = y - \eta \qquad (A.3)$$

$$z_0 = z - \zeta \qquad (A.4)$$

The symbol $\oint\!\!\!\!\!\!\int$ means that the integral in Equation (A.1) is defined in the sense of its "finite part" (Ref. 17).

Rodemich (Ref. 7) has derived an expression for the kernel function for a nonplanar surface in the form

$$K = e^{-i\omega x_0/U_\infty}(K_1 T_1/r^2 + K_2 T_2^*/r^4) \qquad (A.5)$$

where

$$r = (y_0^2 + z_0^2)^{1/2} \qquad (A.6)$$

$$T_1 = \cos(\gamma_r - \gamma_s) \qquad (A.7)$$

$$T_2^* = (z_0 \cos \gamma_r - y_0 \sin \gamma_r)(z_0 \cos \gamma_s - y_0 \sin \gamma_s) \qquad \text{(A. 8)}$$

(N. B., the definition of T_2^* in Equations (A. 5) and (A. 8) differs from that of T_2 in Refs. 7 and 8 by the factor r^2.)

and Landahl[8] has simplified the forms of K_1 and K_2 to read

$$K_1 = I_1 + [Mr/R]\left[e^{-ik_1 u_1}/(1+u_1^2)^{1/2}\right] \qquad \text{(A. 9)}$$

$$K_2 = -3I_2 - \frac{ik_1 M^2 r^2}{R^2} \frac{e^{-ik_1 u_1}}{(1+u_1^2)^{1/2}} - \frac{Mr_1}{R}\left[(1+u_1^2)\frac{\beta^2 r^2}{R^2} + 2 + \frac{Mr\, u_1}{R}\right]\frac{e^{-ik_1 u_1}}{(1+u_1^2)^{3/2}} \qquad \text{(A. 10)}$$

where

$$u_1 = (MR - x_0)/\beta^2 r \qquad \text{(A. 11)}$$

$$k_1 = \omega r / U_\infty \qquad \text{(A. 12)}$$

$$\beta = (1 - M^2)^{1/2} \qquad \text{(A. 13)}$$

$$R = (x_0^2 + \beta^2 r^2)^{1/2} \qquad \text{(A. 14)}$$

and

$$I_1(u_1, k_1) = \int_{u_1}^{\infty} \frac{e^{-ik_1 u}}{(1+u^2)^{3/2}}\, du \qquad \text{(A. 15)}$$

$$I_2(u_1, k_1) = \int_{u_1}^{\infty} \frac{e^{-ik_1 u}}{(1+u^2)^{5/2}}\, du \qquad \text{(A. 16)}$$

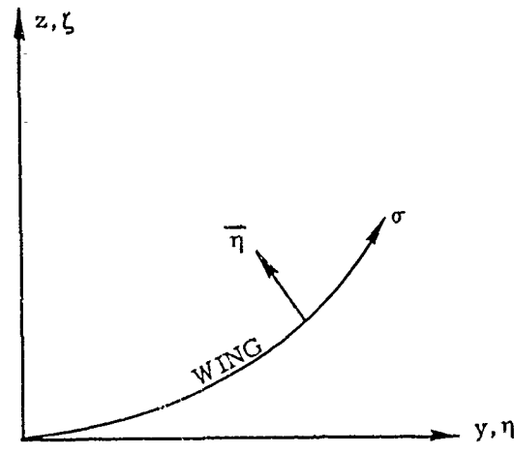

Figure A-1

At zero frequency the planar part of the kernel is

$$K_1^{(s)} = I_1 + \frac{Mr}{R} \quad \frac{1}{(1+u_1^2)^{1/2}} \qquad \text{(A. 17)}$$

where

$$I_1 = \int_{u_1}^{\infty} \frac{du}{(1+u^2)^{3/2}} \qquad \text{(A. 18a)}$$

$$= 1 - u_1 (1 + u_1^2)^{-1/2} \qquad \text{(A. 18b)}$$

so that

$$K_1^{(s)} = 1 + x_0/R \qquad \text{(A. 19)}$$

The zero frequency value of the nonplanar part of the kernel is easily found from the planar part (Refs. 7 and 8).

$$K_2 = r^3 \frac{\partial}{\partial r} \left(\frac{1}{r} \frac{\partial I_0}{\partial r} \right) \tag{A.20}$$

where

$$\frac{\partial I_0}{\partial r_1} = K_1 / r \tag{A.21}$$

so that

$$K_{20} = r^3 \frac{\partial}{\partial r} \left[\frac{1}{r^2} \left(1 + \frac{x_0}{R} \right) \right] \tag{A.22a}$$

$$= - 2 - (x_0/R) (2 + \beta^2 r^2 / R^2) \tag{A.22b}$$

Although the integrals I_1 and I_2 [Equations (A.15) and (A.16)] are easily evaluated at zero frequency, no explicit solution is possible for nonzero frequency. However, the symmetry properties of the integrands permit consideration of only nonnegative arguments u_1 since, for $u_1 < 0$, we note that

$$I_1 (u_1, k_1) = 2 \mathrm{Re} I_1 (0, k_1) - \mathrm{Re} I_1 (-u_1, k_1) + i \mathrm{Im} I_1 (-u_1, k_1) \tag{A.23}$$

and

$$I_2 (u_1, k_1) = 2 \mathrm{Re} I_2 (0, k_1) - \mathrm{Re} I_2 (-u_1, k_1) + i \mathrm{Im} I_2 (-u_1, k_1) \tag{A.24}$$

The integration of I_1 by parts once gives

$$I_1(u_1, k_1) = e^{-ik_1u_1}\left[1 - u_1(1+u_1^2)^{-1/2} - ik_1 I_0(u_1, k_1)\right] \tag{A.25}$$

where

$$I_0(u_1, k_1) = e^{ik_1u_1}\int_{u_1}^{\infty}\left[1 - u(1+u^2)^{-1/2}\right]e^{-ik_1u}\,du \tag{A.26}$$

Integrating I_2 by parts twice leads to

$$3I_2(u_1, k_1) = e^{-ik_1u_1}\left\{(2+ik_1u_1)\left[1 - u_1(1+u_1^2)^{-1/2}\right]\right. \tag{A.27}$$

$$\left. - u_1(1+u_1^2)^{-3/2} - ik_1 I_0(u_1, k_1) + k_1^2 J_0(u_1, k_1)\right\}$$

where

$$J_0(u_1, k_1) = e^{ik_1u_1}\int_{u_1}^{\infty} u\left[1 - u(1+u^2)^{-1/2}\right]e^{-ik_1u}\,du \tag{A.28}$$

The integrals I_0 and J_0 can be evaluated using approximations to $u(1+u^2)^{-1/2}$ Laschka[18] has obtained an extremely accurate approximation in exponential form for $u \geq 0$

$$1 - u(1+u^2)^{-1/2} \approx \sum_{n=1}^{11} a_n e^{-ncu} \tag{A.29}$$

where $c = 0.372$ and the a_n are given in Table I. The maximum error of this approximation is 0.135%. The integrals J_0 and J_0 for $u \geq 0$ then become

$$I_0(u_1, k_1) \approx \sum_{n=1}^{11} \frac{a_n e^{-ncu_1}}{n^2c^2 + k_1^2}(nc - ik_1) \tag{A 30}$$

and

$$J_0(u_1, k_1) \approx \sum_{n=1}^{11} \frac{a_n e^{-ncu_1}}{(n^2c^2 + k_1^2)^2} \left\{ n^2c^2 - k_1^2 \right.$$

(A. 31)

$$\left. + ncu_1(n^2c^2 + k_1^2) - ik[2nc + u_1(n^2c^2 + k_1^2)] \right\}$$

The desired integrals I_1 and I_2 then follow from Equations (A. 25) and (A. 27) for $u_1 \geq 0$, and from Equations (A. 23)-(A. 25) and (A. 27) for $u_1 < 0$.

Table I - Coefficients in Laschka's Approximation to $u(1 + u^2)^{-1/2}$

n	a_n
1	+ 0.24186198
2	- 2.7918027
3	+ 24.991079
4	- 111.59196
5	+ 271.43549
6	- 305.75288
7	- 41.183630
8	+ 545.98537
9	- 644.78155
10	+ 328.72755
11	- 64.279511

APPENDIX B. INCREMENTAL OSCILLATORY DOWNWASH FACTORS

The planar part of the incremental downwash factor is approximated by

$$D^{(1)}_{rs} = \frac{\Delta x_s}{8\pi} \int_{-e}^{e} \frac{P_1(\bar{\eta})}{(\bar{y}-\bar{\eta})^2 + \bar{z}^2} \, d\bar{\eta} \qquad \text{(B. 1)}$$

where $P_1(\bar{\eta})$ is the parabolic approximation

$$P_1(\bar{\eta}) = A_1\bar{\eta}^2 + B_1\bar{\eta} + C_1 \qquad \text{(B. 2a)}$$

$$\approx \{K_1 \exp[-i\omega(\bar{x}-\bar{\eta}\tan\lambda_s)/U] - K_1^{(s)}\} T_1 \qquad \text{(B. 2b)}$$

If we denote the inboard, center, and outboard values of $P_1(\bar{\eta})$ by $P_1(-e)$, $P_1(0)$, and $P_1(e)$, respectively, the parabolic coefficients are

$$A_1 = [P_1(-e) - 2P_1(0) + P_1(e)]/2e^2 \qquad \text{(B. 3)}$$

$$B_1 = [P_1(e) - P_1(-e)]/2e \qquad \text{(B. 4)}$$

$$C_1 = P_1(0) \qquad \text{(B. 5)}$$

The integral of Eq. (B. 1) is given in Ref. 1. However, some discussion of the integral

$$F = \int_{-e}^{e} \frac{d\bar{\eta}}{(\bar{y}-\bar{\eta})^2 + \bar{z}^2} \qquad \text{(B. 6a)}$$

$$= \frac{1}{|\bar{z}|} \tan^{-1} \frac{2e\,|\bar{z}|}{\bar{y}^2 + \bar{z}^2 - e^2} \qquad \text{(B. 6b)}$$

is warranted. The value of the arctangent is taken in the range $(-\pi \rightarrow +\pi)$. When $\bar{y}^2 + \bar{z}^2 \geq e^2$, Equation B.6b is well behaved and approaches zero as z approaches zero. Under these circumstances it is convenient to introduce a parameter α defined by

$$F = \frac{2e}{\bar{y}^2 + \bar{z}^2 - e^2} \left(1 - \alpha \frac{\bar{z}^2}{e^2}\right) \tag{B.7}$$

where

$$\alpha \approx \frac{4e^4}{(\bar{y}^2 + \bar{z}^2 - e^2)^2} \sum_{n=2}^{7} \frac{(-1)^n}{2n-1} \left(\frac{2e\bar{z}}{\bar{y}^2 + \bar{z}^2 - e^2}\right)^{2n-4} \tag{B.8}$$

Eq. (B.8) has been used for $|2e\bar{z}/(\bar{y}^2 + \bar{z}^2 - e^2)| \leq 0.3$ when $\bar{y}^2 + \bar{z}^2 > e^2$. Then the planar downwash factor becomes

$$D_{rs}^{(1)} = \frac{\Delta x_s}{8\pi} \left\{ [(\bar{y}^2 - \bar{z}^2) A_1 + \bar{y} B_1 + C_1] F + (\tfrac{1}{2} B_1 + \bar{y} A_1) \log \frac{(\bar{y}-e)^2 + \bar{z}^2}{(\bar{y}+e)^2 + \bar{z}^2} + 2eA_1 \right\} \tag{B.9}$$

The incremental nonplanar oscillatory downwash factor is approximated by

$$D_{rs}^{(2)} = \frac{\Delta x_s}{8\pi} \oint_{-e}^{e} \frac{P_2(\bar{\eta})}{[(\bar{y}-\bar{\eta})^2 + \bar{z}^2]^2} \, d\bar{\eta} \tag{B.10}$$

where $P_2(\bar{\eta})$ is another parabolic approximation

$$P_1(\bar{\eta}) = A_2\bar{\eta}^2 + B_2\bar{\eta} + C_2 \tag{B.11a}$$

$$\approx \{K_2 \exp[-i\omega(\bar{x}-\bar{\eta}\tan\lambda_s)/U] - K_2^{(s)}\} T_2^* \tag{B.11b}$$

Letting $P_2(-e)$, $P_2(0)$, and $P_2(e)$ denote the inboard, center, and outboard values of $P_2(\bar{\eta})$, respectively, we have

$$A_2 = [P_2(-e) - 2P_2(0) + P_2(e)]/2e^2 \tag{B.12}$$

$$B_2 = [P_2(e) - P_2(-e)]/2e \tag{B.13}$$

$$C_2 = P_2(0) \tag{B.14}$$

The nonplanar downwash factor is then evaluated to be

$$D_{2rs} = \frac{\Delta x_s}{16\pi\bar{z}^2} \left\{ \left[(\bar{y}^2+\bar{z}^2)A_2 + \bar{y}B_2 + C_2\right] F \right. \tag{B.15}$$

$$+ \frac{1}{(\bar{y}+e)^2 + \bar{z}^2} \left([(\bar{y}^2+\bar{z}^2)\bar{y} + (\bar{y}^2-\bar{z}^2)e]A_2 + (\bar{y}^2+\bar{z}^2+\bar{y}e)B_2 + (\bar{y}+e)C_2 \right)$$

$$\left. - \frac{1}{(\bar{y}-e)^2 + \bar{z}^2} \left([(\bar{y}^2+\bar{z}^2)\bar{y} - (\bar{y}^2-\bar{z}^2)e]A_2 + (\bar{y}^2+\bar{z}^2-\bar{y}e)B_2 + (\bar{y}-e)C_2 \right) \right\}$$

Eq. (B.15) tends to lose significance for small values of $\bar{z}$. Introducing α into Eq. (B.15) thru Eq. (B.7) leads to

$$D_{rs}^{(2)} = \frac{\Delta x_s}{8\pi(\bar{y}^2+\bar{z}^2-e^2)} \left\{ \frac{2(\bar{y}^2+\bar{z}^2+e^2)\,(e^2A_2+C_2) + 4\bar{y}e^2 B_2}{[(\bar{y}-e)^2+\bar{z}^2][(\bar{y}-e)^2+\bar{z}^2]} \right.$$

$$\left. - \frac{\alpha}{e^2}\,[(\bar{y}^2+\bar{z}^2)A_2 + \bar{y}B_2 + C_2] \right\} \qquad \text{(B.16)}$$

The simplification of Eq. (B.15) via Eq. (B.7) is somewhat tedious but results in the more accurate form above in which α is again given by Eq. (B.8). Eq. (B.16) has been used in general except when $|(\bar{y}^2+\bar{z}^2-e^2)/2e\bar{z}| \leq 0.1$ in which case Eq. (B.15) is used.

When $\bar{y}^2 + \bar{z}^2 < e^2$ then the expression for F is not well behaved but approaches infinity as $z \to 0$. The specific behavior is

$$\lim_{\bar{z}\to 0} \quad F \to \pi/|\bar{z}| \,, \quad \text{for } \bar{y}^2 + \bar{z}^2 < e^2$$

Under these circumstances it can be shown that the term

$$\lim_{\bar{z}\to 0} \quad F \left\{ C_1 + \bar{y}B_1 + (\bar{y}^2-\bar{z}^2)A_1 + \frac{1}{2\bar{z}^2}\,(C_2+\bar{y}B_2+(\bar{y}^2+\bar{z}^2)A_2) \right\}$$

$$\to 0$$

even as $F \to \infty$. Numerically, of course, this expression will lose accuracy at some value of $\bar{z}$. An example calculation has shown that for $\frac{x-\xi}{c} = 0.5$, $k = 6.0$ and $e = 1/120$, the gap, $\bar{z}/e$, at which numerical difficulties arose was 0.0025. Since e is small $\bar{z} = e\,(.0025)$ is very small and can be assumed to be zero; i.e., the planar case.

APPENDIX C. THE STEADY NONPLANAR DOWNWASH FACTOR

The steady nonplanar downwash factor is

$$D_{rs}^{(s)} = (\Delta x_s / 8\pi) \oint_{-e}^{e} \left(\frac{K_1^{(s)} T_1}{r^2} + \frac{K_2^{(s)} T_2^*}{r^4} \right) d\eta \qquad (C.1)$$

The downwash factor has been given by Hedman (Ref. 2, App. C) and is equivalent to Equation (C. 1), although it is derived from fundamental vortex considerations rather than evaluating the integral in Equation (C. 1). We find it convenient to rederive Hedman's results in order to facilitate the programming of the equations.

The vector geometry for a finite-length, constant-strength vortex is shown in Figure C-1. The vector form of the Biot-Savart Law for this segment is

$$\vec{V} = \frac{\vec{\Gamma} \times \vec{d}}{4\pi d^2} (\cos\theta - \cos\varphi) \qquad (C\ 2)$$

where

$$\vec{d} = \vec{R}_1 - (\vec{\Gamma}/\Gamma) R_1 \cos\theta \qquad (C\ 3)$$

$$\cos\theta = (\vec{R}_1/R_1) \cdot (\vec{\Gamma}/\Gamma) \qquad (C.4)$$

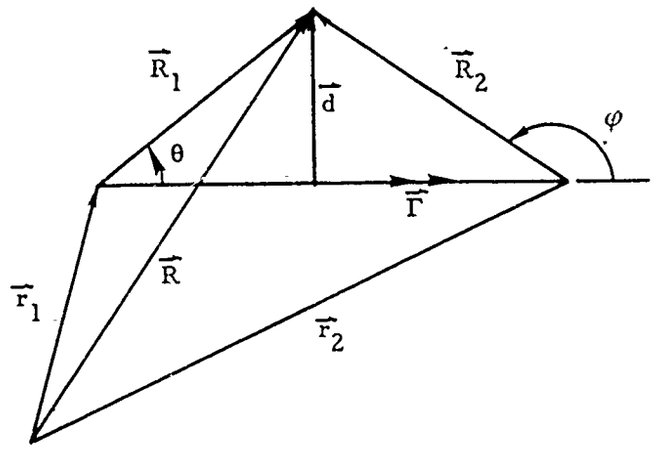

Figure C. 1

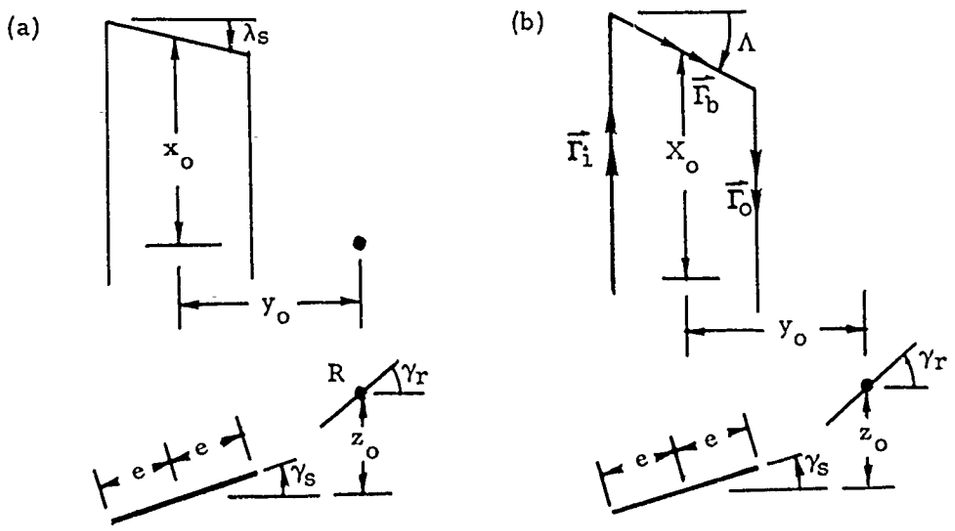

Figure C. 2

and

$$\cos \varphi = (\vec{R}_2/R_2) \cdot (\vec{\Gamma}/\Gamma) \tag{C.5}$$

and where an arrow indicates a vector. The normalwash at the receiving point, where the dihedral angle is γ_r, is

$$w = \vec{V} \cdot (\vec{j} \sin \gamma_r - \vec{k} \cos \gamma_r) \tag{C.6}$$

where

$$\vec{V} = \vec{j} V_y + \vec{k} V_z \tag{C.7}$$

The general result desired for a horseshoe vortex system applies the foregoing equations to the bound and two trailing vortex components of the horseshoe system.

The physical geometry of a horseshoe vortex system is shown in Figure C.2(a); the geometry modified by the Prandt-Glauert Transformation is shown in Figure C.2(b). The transformations are

$$X_0 = x_0/\beta \tag{C.8}$$

and

$$\tan \Lambda = (\tan \gamma_s)/\beta \tag{C.9}$$

The Biot-Savart Law is to be applied using the geometry of Figure C.2(b). Let the origin of coordinates be the center of the bound vortex. Then the distance to the receiving point (X_0, y_0, z_0) is

$$\vec{R} = \vec{i} X_0 + \vec{j} y_0 + \vec{k} z_0 \tag{C.10}$$

and the distances from the inboard and outboard ends of the bound vortex are

$$\vec{r}_i = -e\,(\vec{i}\tan\Lambda + \vec{j}\cos\gamma_s + \vec{k}\sin\gamma_s) \qquad (C.11)$$

and

$$\vec{r}_o = e\,(\vec{i}\tan\Lambda + \vec{j}\cos\gamma_s + \vec{k}\sin\gamma_s) \qquad (C.12)$$

respectively. The distance to the receiving point from the inboard end is

$$\vec{R}_i = \vec{R} - \vec{r}_i \qquad (C.13a)$$

$$= \vec{i}\,(X_0 + e\tan\Lambda) + \vec{j}\,(y_0 + e\cos\gamma_s) + \vec{k}(z_0 + e\sin\gamma_s) \qquad (C.13b)$$

$$= \vec{i}\,R_{ix} + \vec{j}R_{iy} + \vec{k}R_{iz} \qquad (C.13c)$$

from which

$$R_i = (R_{ix}^2 + R_{iy}^2 + R_{iz}^2)^{1/2} \qquad (C.14)$$

The distance to the receiving point from the outboard end is

$$\vec{R}_o = \vec{R} - \vec{r}_o \qquad (C.15a)$$

$$= \vec{i}(X_0 - e\tan\Lambda) + \vec{j}(y_0 - e\cos\gamma_s) + \vec{k}(z_0 - e\sin\gamma_s) \qquad (C.15b)$$

$$= \vec{i}R_{ox} + \vec{j}R_{oy} + \vec{k}R_{oz} \qquad (C.15c)$$

from which

$$R_o = (R_{ox}^2 + R_{oy}^2 + R_{oz}^2)^{1/2} \qquad (C.16)$$

The vorticity vectors for the three components of the horseshoe vortex complete the basic data required for calculation of the downwash factors.

$$\Gamma_b = \Gamma(\vec{i} \sin\Lambda + \vec{j} \cos\Lambda \cos\gamma_s + \vec{k} \cos\Lambda \sin\gamma_s) \qquad (C.17)$$

$$\Gamma_i = \Gamma(-\vec{i}) \qquad (C.18)$$

$$\Gamma_o = \Gamma(+\vec{i}) \qquad (C.19)$$

We begin the final calculations by finding the cosines of θ and φ and the normal distance vectors $\vec{d}$ for the bound, inboard, and outboard vortices. For the bound vortex,

$$\cos\theta_b = (\vec{R}_i/R_i) \cdot (\vec{\Gamma}_b/\Gamma) \qquad (C.20a)$$

$$= \frac{1}{R_i} (R_{ix} \sin\Lambda + R_{iy} \cos\Lambda \cos\gamma_s + R_{iz} \cos\Lambda \sin\gamma_s) \qquad (C.20b)$$

$$\cos\varphi_b = (\vec{R}_o/R_o) \cdot (\vec{\Gamma}_b/\Gamma) \qquad (C.21a)$$

$$= \frac{1}{R_o} (R_{ox} \sin\Lambda + R_{oy} \cos\Lambda \cos\gamma_s + R_{oz} \cos\Lambda \sin\gamma_s) \qquad (C.21b)$$

$$\vec{d}_b = \vec{R}_i - (\vec{\Gamma}_b/\Gamma) R_i \cos\theta_b \qquad (C.22a)$$

$$= \vec{i}(R_{ix} - R_i \cos\theta_b \sin\Lambda)$$

$$+\vec{j}(R_{iy} - R_i \cos\theta_b \cos\Lambda \cos\gamma_s) \qquad \text{(C. 22b)}$$

$$+\vec{k}(R_{iz} - R_i \cos\theta_b \cos\Lambda \sin\gamma_s)$$

$$= \vec{i}d_{bx} + \vec{j}d_{by} + \vec{k}d_{bz} \qquad \text{(C. 22c)}$$

For the inboard vortex,

$$\cos\theta_i = +1 \qquad \text{(C. 23)}$$

$$\cos\varphi_i = (\vec{R}_i/R_i) \cdot (\vec{\Gamma}_i/\Gamma) \qquad \text{(C. 24a)}$$

$$= -R_{ix}/R_i \qquad \text{(C. 24b)}$$

$$\vec{d}_i = \vec{j}R_{iy} + \vec{k}R_{iz} \qquad \text{(C. 25)}$$

Finally, for the outboard vortex,

$$\cos\theta_o = (\vec{R}_o/R_o) \cdot (\vec{\Gamma}_o/\Gamma) \qquad \text{(C. 26a)}$$

$$= R_{ox}/R_o \qquad \text{(C. 26b)}$$

$$\cos\varphi_o = -1 \qquad \text{(C. 27)}$$

$$\vec{d}_o = \vec{j}R_{oy} + \vec{k}R_{oz} \qquad \text{(C. 28)}$$

We next evaluate the velocity induced by each of the three vortices. The bound vortex induces the velocity

$$\vec{V}_b = \frac{\vec{\Gamma}_b \times \vec{d}_b}{4\pi d_b^2} (\cos\theta_b - \cos\varphi_b) \qquad \text{(C. 29a)}$$

$$= \frac{\Gamma}{4\pi d_b^2}(\cos\theta_b - \cos\varphi_b)\,[\vec{i}\,(d_{bz}\cos\Lambda\cos\gamma_s - d_{by}\cos\Lambda\sin\gamma_s)$$

$$+ \vec{j}(d_{bx}\cos\Lambda\sin\gamma_s - d_{bz}\sin\Lambda) \qquad \text{(C.29b)}$$

$$+ \vec{k}(d_{by}\sin\Lambda - d_{bx}\cos\Lambda\cos\gamma_s)\,]$$

$$= \Gamma(\vec{i}V_{bx} + \vec{j}V_{by} + \vec{k}V_{bz}) \qquad \text{(C.29c)}$$

where

$$d_b^2 = d_{bx}^2 + d_{by}^2 + d_{bz}^2 \qquad \text{(C.30)}$$

The inboard vortex induces the velocity

$$\vec{V}_i = \frac{\vec{r}_i \times \vec{d}_i}{4\pi d_i^2}(\cos\theta_i - \cos\varphi_i) \qquad \text{(C.31a)}$$

$$= \frac{\Gamma(1 - \cos\varphi_i)}{4\pi R_{iy}^2 + R_{iz}^2}(\vec{j}R_{iz} - \vec{k}R_{iy}) \qquad \text{(C.31b)}$$

$$= \Gamma(\vec{j}V_{iy} + \vec{k}V_{iz}) \qquad \text{(C.31c)}$$

and the outboard vortex induces the velocity

$$\vec{V}_o = \frac{\vec{\Gamma}_o \times \vec{d}_o}{4\pi d_o^2}(\cos\theta_o - \cos\varphi_o) \qquad \text{(C.32a)}$$

$$= \frac{\Gamma}{4\pi}\frac{(\cos\theta_o - 1)}{(R_{oy}^2 + R_{oz}^2)}(-\vec{j}R_{oz} + \vec{k}R_{oy}) \qquad \text{(C.32b)}$$

$$= \Gamma(\vec{j}V_{oy} + \vec{k}V_{oz}) \qquad \text{(C.32c)}$$

The total velocity induced by the horseshoe vortex is

$$\vec{V} = \vec{V}_b + \vec{V}_i + \vec{V}_o \qquad \text{(C. 33a)}$$

$$= \Gamma[\vec{i}\,(V_{bx} + V_{ix} + V_{ox}) + \vec{j}(V_{by} + V_{iy} + V_{oy})$$

$$+ \vec{k}(V_{bz} + V_{iz} + V_{oz})\,] \qquad \text{(C 33b)}$$

$$= \Gamma(\vec{i}V_x + \vec{j}V_y + \vec{k}V_z) \qquad \text{(C. 33c)}$$

The normalwash velocity is then given by

$$w = \vec{V} \cdot (\vec{j} \sin \gamma_r - \vec{k} \cos \gamma_r) \qquad \text{(C. 34a)}$$

$$= \Gamma(V_y \sin \gamma_r - V_z \cos \gamma_r) \qquad \text{(C. 34b)}$$

which leads, finally, to the steady nonplanar downwash factor

$$D^{(s)}_{rs} = \Delta x_s w_r / 2\Gamma \qquad \text{(C. 35a)}$$

$$= (V_y \sin \gamma_r - V_z \cos \gamma_r)\ \Delta x_s / 2 \qquad \text{(C. 35b)}$$

A numerical difficulty arises when the receiving point is on an extension of the bound vortex axis. The limit of V_b as d_b approaches zero is also zero. Numerical accuracy can be preserved by utilizing a series expansion of $(\cos \theta_b - \cos \varphi_b)$. For small θ_b and φ_b

$$\cos \theta_b - \cos \varphi_b \approx (\varphi_b^2 - \theta_b^2)\ /\ 2 \qquad \text{(C. 36)}$$

where

$$\varphi_b \approx d_b / R_o \tag{C.37}$$

and

$$\theta_b \approx d_b / R_i \tag{C.38}$$

so that

$$(\cos \theta_b - \cos \varphi_b) / d_b^2 \approx \frac{1}{2} \left(\frac{1}{R_o^2} - \frac{1}{R_i^2} \right) \tag{C.39}$$

If the angles are close to π

$$(\cos \theta_b - \cos \varphi_b) / d_b^2 \approx \frac{1}{2} \left(\frac{1}{R_i^2} - \frac{1}{R_o^2} \right) \tag{C.40}$$

In either case

$$(\cos \theta_b - \cos \varphi_b) / d_b^2 \approx \frac{1}{2} \left| \frac{1}{R_i^2} - \frac{1}{R_o^2} \right| \tag{C.41}$$

The program uses the approximation if max ($|\cos \theta_b|$, $|\cos \varphi_b|$) > 0.999. If $\theta_b \approx 0$ and $\varphi_b \approx \pi$, the receiving point is close to the bound vortex This case is only of interest in induced drag calculations. Then the bound vortex induces no velocity on itself. The program sets $(\cos \theta_b - \cos \varphi_b) / d_b^2$ to zero if $\cos \theta_b \cos \varphi_b < 0$ and max ($|\cos \theta_b|$, $|\cos \varphi_b|$) > 0.999.

APPENDIX D. THE SUBSTANTIAL DERIVATIVE AND INTEGRATION MATRICES

D.1 The First Alternative

Alternative No. 1 for the substantial derivative matrix [W] and the integration matrix [B] assumes that the deflections of a given spanwise division (aerodynamic strip) can be determined by the following degrees of freedom.

- h - plunging of strip
- α - pitching of strip
- β - rotation of primary control surface
- δ - rotation of secondary control surface
- $\bar{\beta}$ - plunging of primary control surface
- $\bar{\delta}$ - plunging of secondary control surface

To describe the format of the matrices involved, we assume that a spanwise division (strip) is idealized into 10 chordwise boxes as shown in Figure D-1. Any number of boxes may be chosen; 10 are used only as an example. The local deflection mode shapes corresponding to the local degrees of freedom h, α, β, δ, $\bar{\beta}$, and $\bar{\delta}$ are also shown in Figure D-1. The [W] and [B] matrices are constructed from the following equations.

$$\left.\begin{aligned} h_j &= h + (x_j - x_1)\alpha \qquad (D.1\text{-}1) \\ \frac{dh_j}{dx} &= \alpha \qquad (D.1\text{-}2) \end{aligned}\right\} x_j < x_2$$

$$\left.\begin{aligned} h_j &= h + (x_j - x_1)\alpha + (x_j - x_3)\beta + \bar{\beta} \qquad (D.1\text{-}3) \\ \frac{dh_j}{dx} &= \alpha + \beta \qquad (D.1\text{-}4) \end{aligned}\right\} x_2 < x_j < x_4$$

$$\left.\begin{aligned} h_j &= h + (x_j - x_1)\alpha + (x_j - x_3)\beta + \bar{\beta} \\ &\quad + (x_j - x_4)\delta + \bar{\delta} \qquad (D.1\text{-}5) \\ \frac{dh_j}{dx} &= \alpha + \beta + \delta \qquad (D.1\text{-}6) \end{aligned}\right\} x_j > x_4$$

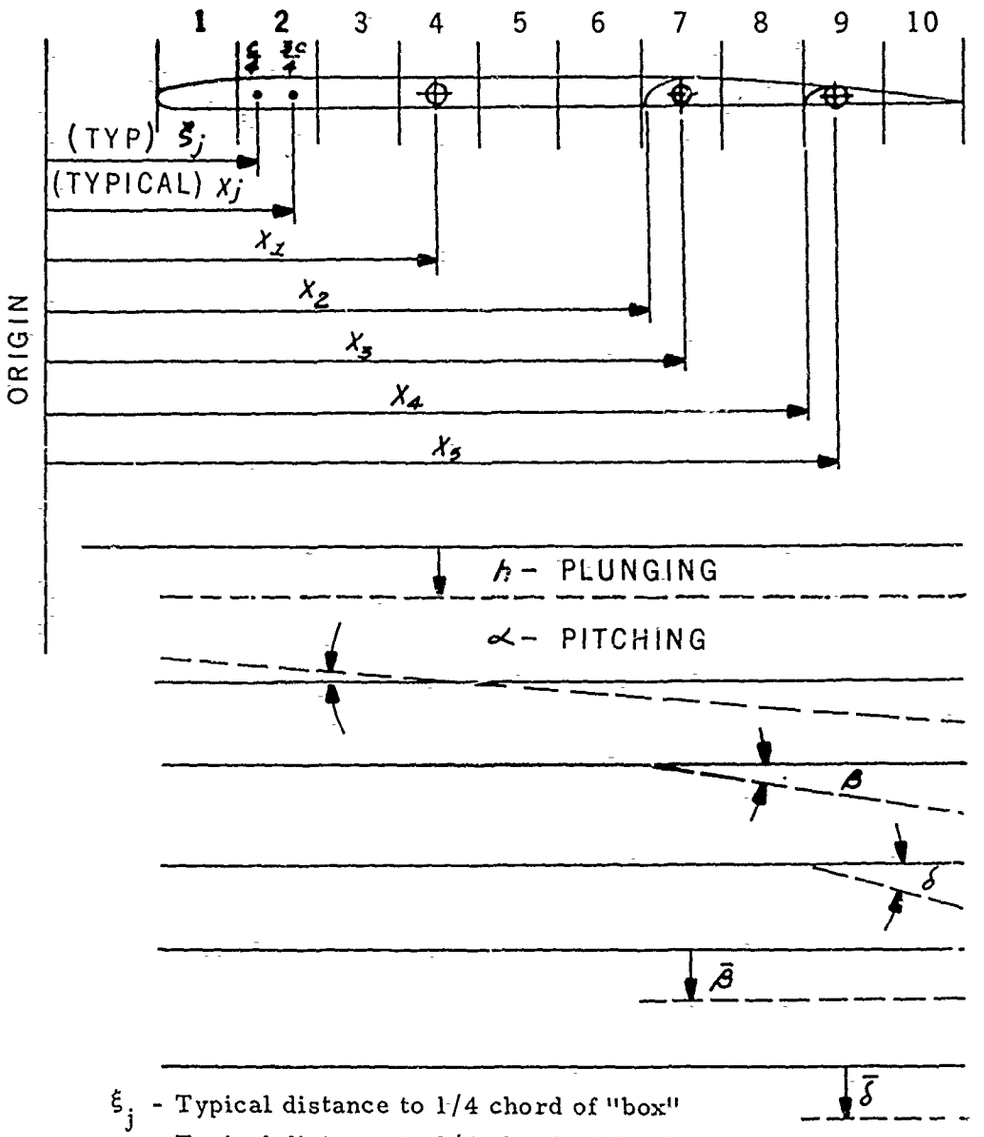

ξ_j - Typical distance to 1/4 chord of "box"

x_j - Typical distance to 3/4 chord of "box"

x_1 - Distance to reference axis

x_2 - Distance to leading edge of primary control surface

x_3 - Distance to hinge line of primary control surface

x_4 - Distance to leading edge of secondary control surface

x_5 - Distance to hinge line of secondary control surface

Figure D-1. Strip Geometry and Local Deflection Shapes for Alternative 1

The format of the [W] matrix which results from the above equations for the example of Figure D-1 is shown in Table D-1. The format of the [B] matrix is not shown, but can be determined by substituting ξ_j for x_j in the [W] matrix and writing

$$[B] = \frac{b_r}{k_r} \quad I\,m\,[W]^T \Big) \lceil A \rfloor \qquad (D.1\text{-}7)$$

where $\lceil A \rfloor$ is the diagonal matrix of box areas. The expression q [B], then represents lifts due to h, $\bar{\beta}$, $\bar{\delta}$, and moments (about x_1, x_3, x_5) due to α, β, δ.

The present version of H7WC generates AIC's only for lifting surfaces; fuselage elements or bays are ignored. (See Part I, Vol II).

TABLE D-1. MATRIX [W] FOR TYPICAL STRIP

ALTERNATIVE NO. 1

	h	α	β	δ	$\bar{\beta}$	$\bar{\delta}$
1	$i\,\frac{k_r}{b_r}$	$1.0 + i\,\frac{k_r}{b_r}(x_j - x_1)$	0	0	0	0
2			0	0	0	0
3			0	0	0	0
4			0	0	0	0
5			0	0	0	0
6			0	0	0	0
7			$1.0 + i\,\frac{k_r}{b_r}(x_j - x_3)$	0	$i\,\frac{k_r}{b_r}$	0
8				0		0
9				$1.0 + i\,\frac{k_r}{b_r}(x_j - x_5)$		$i\,\frac{k_r}{b_r}$
10	$i\,\frac{k_r}{b_r}$	$1.0 + i\,\frac{k_r}{b_r}(x_j - x_1)$	$1.0 + i\,\frac{k_r}{b_r}(x_j - x_3)$	$1.0 + i\,\frac{k_r}{b_r}(x_j - x_5)$	$i\,\frac{k_r}{b_r}$	$i\,\frac{k_r}{b_r}$

D.2 The Second Alternative

Alternative No. 2 which includes parabolic camber is shown in Figure D-2. The Lagrangian interpolation formulas are used to describe the deflections of the strip. The applicable formulas are:

$$h_j = \frac{(x_j - x_2)(x_j - x_3)}{(x_1 - x_2)(x_1 - x_3)} h_1 + \frac{(x_j - x_1)(x_j - x_3)}{(x_2 - x_1)(x_2 - x_3)} h_2 + \frac{(x_j - x_1)(x_j - x_2)}{(x_3 - x_1)(x_3 - x_2)} h_3, \begin{cases} x_j < x_3 \text{ when control surface is present;} \\ \text{all } x_j \text{ with no control surface.} \end{cases} \quad (D.2\text{-}1)$$

$$\frac{dh_j}{dx} = \left(\frac{(x_j - x_2)+(x_j - x_3)}{(x_1 - x_2)(x_1 - x_3)}\right) h_1 + \left(\frac{(x_j - x_1)+(x_j - x_3)}{(x_2 - x_1)(x_2 - x_3)}\right) h_2 + \left(\frac{(x_j - w_1)+(x_j - x_2)}{(x_3 - x_1)(x_3 - x_2)}\right) h_3, \begin{cases} x_j < x_3 \text{ when control surface is present;} \\ \text{all } x_j \text{ with no control surface.} \end{cases} \quad (D.2\text{-}2)$$

When the control surfaces are present, we assume that the deflections aft of x_3 can be determined by linear extrapolation. We then have

$$h_j = \left(\frac{(x_3 - x_2)(x_j - x_3)}{(x_3 - x_1)(x_1 - x_2)}\right) h_1 + \left(\frac{(x_3 - x_1)(x_j - x_3)}{(x_2 - x_1)(x_2 - x_3)}\right) h_2 + \left(1 + \left(\frac{(x_3 - x_1)+(x_3 - x_2)}{(x_3 - x_1)(x_3 - x_2)}\right)(x_j - x_3)\right) h_3, \; x_j > x_3 \quad (D.2\text{-}3)$$

$$\frac{\partial h_j}{\partial x} = h_1 \frac{(x_3 - x_2)}{(x_1 - x_2)(x_1 - x_3)} + h_2 \frac{(x_3 - x_1)}{(x_2 - x_1)(x_2 - x_3)} + h_3 \frac{(x_3 - x_1)+(x_3 - x_2)}{(x_3 - x_1)(x_3 - x_2)}, \; x_j > x_3 \quad (D.2\text{-}4)$$

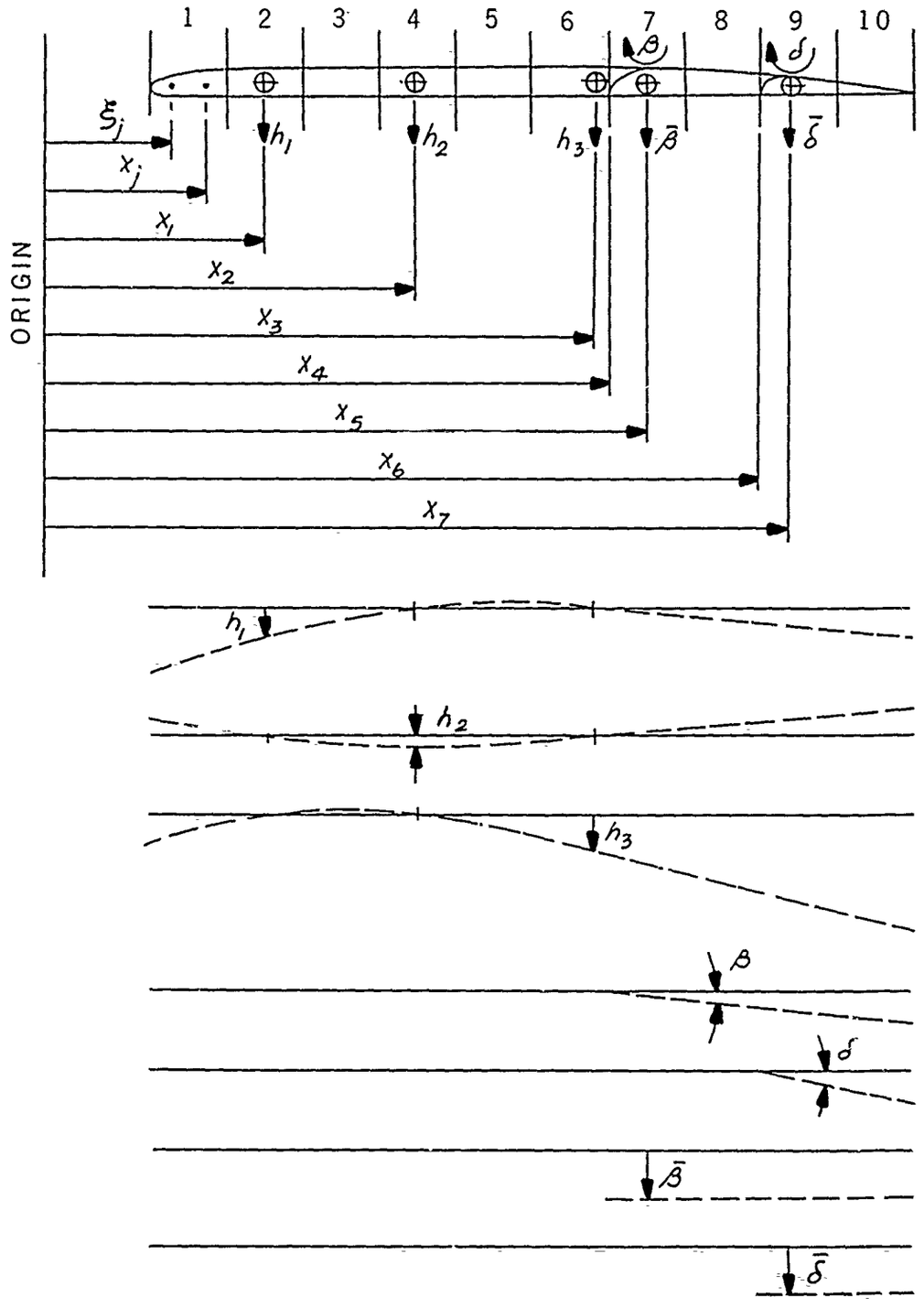

Figure D-2. Strip Geometry and Local Deflection Shapes for Alternative 2.

The incremental deflections due to the control surface degrees of freedom are given by the equations below.

$$\Delta_1 h_j = (x_j - x_5)\,\beta, \qquad x_j > x_4 \tag{D.2-5}$$

$$\frac{\partial(\Delta_1 h_j)}{\partial x} = \beta, \qquad x_j > x_4 \tag{D.2-6}$$

$$\Delta_2 h_j = (x_j - x_7)\,\delta, \qquad x_j > x_7 \tag{D.2-7}$$

$$\frac{\partial(\Delta_2 h_j)}{\partial x} = \delta, \qquad x_j > x_7 \tag{D.2-8}$$

$$\Delta_3 h_j = \bar{\beta}, \qquad x_j > x_4 \tag{D.2-9}$$

$$\Delta_4 h_j = \bar{\delta}, \qquad x_j > x_7 \tag{D.2-10}$$

The [W] and [B] matrices can now be constructed from Equations (D.2-1) through (D.2-10). Figure D-2 indicates in a qualitative manner the local deflection mode shapes corresponding to the degrees of freedom shown.

Unclassified

Security Classification

DOCUMENT CONTROL DATA - R & D

(Security classification of title, body of abstract and indexing annotation must be entered when the overall report is classified)

1. ORIGINATING ACTIVITY (Corporate author)	2a. REPORT SECURITY CLASSIFICATION
Douglas Aircraft Company Aircraft Division	Unclassified
	2b. GROUP

3. REPORT TITLE

Subsonic Unsteady Aerodynamics for General Configurations
Part I, Vol I - Direct Application of the Nonplanar Doublet-Lattice Method

4. DESCRIPTIVE NOTES (Type of report and inclusive dates)

Final Technical Report, December 1969 - September 1970

5. AUTHOR(S) (First name, middle initial, last name)

J.P. Giesing
T.P. Kalman
W.P. Rodden

6. REPORT DATE	7a. TOTAL NO. OF PAGES	7b. NO OF REFS
November 1971	76	18

8a. CONTRACT OR GRANT NO.	9a. ORIGINATOR'S REPORT NUMBER(S)
F33615-70-C-1167	
b. PROJECT NO. 1370	MDC-J0944
c. Task No. 137003	9b. OTHER REPORT NO(S) (Any other numbers that may be assigned this report)
d.	AFFDL-TR-71-5, Part I, Vol I

10. DISTRIBUTION STATEMENT

Distribution limited to U.S. Government agencies only; test and evaluation; statement applied 23 June 1971. Other requests for this document must be referred to AF Flight Dynamics Laboratory (FY), Wright-Patterson AFB, Ohio 45433.

11. SUPPLEMENTARY NOTES	12. SPONSORING MILITARY ACTIVITY
	Air Force Flight Dynamics Laboratory Wright-Patterson Air Force Base, Ohio 45433

13. ABSTRACT

Two methods of accounting for body-lifting surface interference in unsteady flow are considered. The first method (Part I) is a direct application of nonplanar lifting surface elements to both the lifting surfaces and the body surfaces. This type of idealization must be used with an axial doublet introduced to account for body incidence effects. The undesirable effects of the annular wing representation are then reduced. The second approach, described in Part II, uses an image system and an axial singularity system to account for the effects of the bodies.

This report also describes an improvement of the Doublet-Lattice Method of Albano and Rodden. The improvement pertains to wing-tail problems where there exists a small vertical (non-zero) separation between the wing and tail planes. Such problems can now be handled with ease.

The methods described in this report are intended to be used by airplane designers to calculate with improved accuracy, the unsteady aerodynamic pressures that act on a lifting surface being propelled at subsonic speeds. The new feature of these calculations is that the effects on the pressure field induced by interference between the fuselage, for example, and the wing or the wing, pylon and nacelle, are taken into account. These calculations are an essential ingredient of flutter analyses and will improve the confidence level of such calculations in preventing wing-store flutter and flutter of advanced vehicles where fuselages are relatively large, provide some lifting capability and cause noticeable interference effects. The general requirement for such calculations are contained in Military Specification MIL-A-8870A(USAF).

DD FORM 1 NOV 65 1473

Unclassified

Security Classification

Unclassified

Security Classification

14. KEY WORDS	LINK A		LINK B		LINK C	
	ROLE	WT	ROLE	WT	ROLE	WT
Unsteady Aerodynamics						
Subsonic Flow						
Aerodynamic Interference						

*U.S.Government Printing Office: 1971 — 759-080/246

Unclassified

Security Classification